SCIENCE CHINA
Information Sciences

• RESEARCH PAPER •

July 2018, Vol. 61 070221:1–070221:18
https://doi.org/10.1007/s11432-017-9341-y

Special Focus on Advances in Disturbance/Uncertainty Estimation and Attenuation Techniques With Applications

# Nonlinear composite bilateral control framework for n-DOF teleoperation systems with disturbances

Zhenhua ZHAO[1], Jun YANG[1*], Cunjia LIU[2] & Wen-Hua CHEN[2]

[1]*School of Automation, Southeast University, Key Laboratory of Measurement and Control of CSE, Ministry of Education, Nanjing* 210096*, China;*
[2]*Department of Aeronautical and Automotive Engineering, Loughborough University, Loughborough* LE11 3TU*, UK*

Received 29 September 2017/Revised 20 December 2017/Accepted 19 January 2018/Published online 25 May 2018

**Abstract** This paper proposes a new nonlinear composite bilateral control framework for n-degree-of-freedom (n-DOF) teleoperation systems with external disturbances. Different with the existing methods which usually regard the dynamics of the master and slave robots as linear impedance models, the proposed control framework fully considers the nonlinear dynamics of the n-DOF teleoperation systems. Central to the proposed framework is the utilization of nonlinear disturbance observers for estimating the disturbances in master and slave robot systems. The nonlinear composite bilateral controller is constructed by incorporating the disturbance estimations into the nonlinear feedback linearization controller. The proposed control method guarantees satisfactory position tracking performance and desired remote force haptic simultaneously for the n-DOF teleoperation systems with external disturbances. The effectiveness of the proposed control framework is validated by its applications on 2-DOF teleoperation systems.

**Keywords** teleoperation system, nonlinear bilateral control, remote force haptic, disturbance rejection, nonlinear disturbance observer

**Citation** Zhao Z H, Yang J, Liu C J, et al. Nonlinear composite bilateral control framework for n-DOF teleoperation systems with disturbances. Sci China Inf Sci, 2018, 61(7): 070221, https://doi.org/10.1007/s11432-017-9341-y

## 1 Introduction

Teleoperation is the operation to control the positions of a remote manipulator and haptic the forces applied on it [1]. The teleoperation systems extend the operator's sensing and manipulation capability to remote locations and are widely utilized in the cases where humans are unable to perform a certain task (e.g., nuclear waste site and radioactive material management, undersea and outer space exploration [2]), or where operators want to improve semi-autonomous execution of a task (e.g., minimally invasive telesurgery and telerehabilitation [3]). A teleoperation system consists of five parts: human operator, master robot, slave robot, environment and communication channel (see Figure 1). To perform a task in the remote environment, human operator manipulates the local master robot, and then with appropriate control action in master and slave robots (i.e., bilateral control action), the slave robot reproduces the master robot's trajectory in remote site and the master robot displays the slave-environment contact force to human operator. The control objective, namely ideal transparency of the teleoperation systems [4], is to keep the slave robot having the same position with the master robot (i.e., $\boldsymbol{x}_s = \boldsymbol{x}_m$ in Figure 1) and to make sure the contact force applied on the operator by the master robot is the same with that applied on the slave robot by the environment (i.e., $\boldsymbol{f}_h' = \boldsymbol{f}_e$ in Figure 1).

* Corresponding author (email: j.yang84@seu.edu.cn)

 

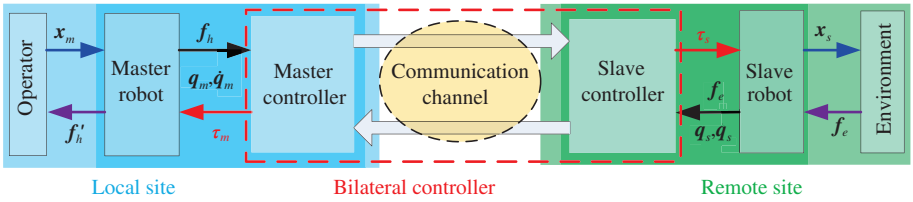


**Figure 1** (Color online) Signal flow of the teleoperation systems.

To be specific, two control tasks should be exactly realized to achieve higher transparency: (1) position control to guarantee the slave robot has the same positions with the master robot; and (2) force control to ensure the operator senses the same force that the environment imposed on the slave robot. Many bilateral control methods have been proposed to improve the transparency of teleoperation systems. Based on the impedance control conception, early researches proposed the two-channel [5] and the four-channel [4, 6] bilateral control architectures. However, satisfactory transparency of these methods is guaranteed only when master and slave robots are linear systems and free from disturbances. Furthermore, the accelerations are generally indispensable for these control approaches [6]. To reduce the effects of nonlinear dynamics in teleoperation systems, a number of elegant nonlinear control methods such as adaptive control [7] and finite-time control methods have been proposed recently [8, 9]. These methods introduce a new way to design the bilateral controller by designing the position tracking controller through nonlinear feedback directly based on the nonlinear dynamics of position tracking errors. However, only the position tracking task is considered in these existing nonlinear dynamics based methods.

To achieve position and force tracking tasks simultaneously and reduce the influence of disturbances, the composite bilateral control methods have been proposed in [10–12] based on linear disturbance observer (LDOB) technique [13]. In [10], the LDOB is employed in work space to estimate the disturbances acting on the master and slave robots, which is called workspace disturbance observer (WDOB) based composite bilateral control method. The estimations based on WDOB are utilized to compensate the disturbances in the master and slave robots such that the systems behave as the desired linear impedance models, and then the WDOB based bilateral controller is developed based on the impedance model. In [11], the WDOB based method is generalized to n-DOF scaling teleopertaion systems. To handle the couplings between the position and force tracking error dynamics encountered by the WDOB based method, the modal space disturbance observer (MDOB) based bilateral control method is proposed in [12]. The modal space control conception is transferring the position and force control tasks into stabilizing the states of modal space (i.e., the differential mode $\boldsymbol{x}_d = \boldsymbol{x}_m - \boldsymbol{x}_s$ and the common mode $\boldsymbol{x}_c = \boldsymbol{f}_h + \boldsymbol{f}_e$ in Figure 1). The MDOB based method utilizes the LDOB to estimate and compensate the disturbances in modal space guaranteeing the states of modal space behave as desired linear dynamics. Thereafter, this composite controller is constructed based on the estimation of MDOB and the nominal linear model. Although the transparency of the teleoperation systems has been improved significantly by above methods, they all set the nominal model of the teleoperation systems as linear impedance models. However, it is well known that, depending on the mechanical configuration, robots may have strong nonlinear dynamics [14, 15] especially for the n-DOF robots. Although some weak nonlinearity may be considered as a part of disturbances and the above existing methods could be applied to yield satisfactory performance, the dynamic performance and transparency of teleoperation systems degrade significantly when master or slave robot exhibits strong nonlinearity.

The nonlinear disturbance observer (NDOB) proposed in [14] is an efficient way to estimate the disturbances in nonlinear systems and it is widely employed in industrial engineering [16–18]. In [19, 20], the NDOB is introduced and designed based on the nonlinear models of the master and slave robots to estimate the disturbances acting on them. Then the NDOB based four-channel bilateral controllers are developed by introducing the disturbance estimations to the baseline four-channel controller. Although this method improves both position and force tracking performance significantly, it needs the acceleration information of the master and slave robots [19] which is usually hard to obtain in practical engineering.

In this paper, a new nonlinear bilateral control framework for the n-DOF teleoperation systems with

external disturbances is developed through the following four steps. First, the nonlinear dynamics of the position and force tracking errors are induced based on the nonlinear dynamics of n-DOF teleopeartion systems. Second, the NDOB is employed to estimate the disturbances in the master and slave robots subsystems. Then, the composite virtual position and force tracking controllers are constructed based on the estimations of NDOB and the nonlinear feedback linearization (NFL) methods. Finally, the real control actions of master and slave robots (i.e., electrical torques) are obtained from the composite virtual controllers through a nonlinear transformation. As compared with the existing methods, the nonlinear composite bilateral control framework has the following major merits: (1) Convergence of both position and force tracking errors are guaranteed simultaneously. (2) Faster convergence rate of position and force tracking errors are achieved due to the direct feedforward compensation of disturbances. (3) Complete decoupling of position and force tracking error dynamics is ensured. Therefore, an improved position and force tracking performance has been achieved in both steady-state and transition.

The rest of this paper is organized as follows. The mathematic model and control objectives of the n-DOF teleoperation systems are given in Section 2. In Section 3, two existing bilateral control methods are analysed and the motivation of our work is highlighted. Section 4 presents the design procedure and the strict stability proof of the proposed nonlinear composite bilateral control framework. Simulation studies are carried out in Section 5. Finally, conclusion is given in Section 6.

## 2 Problem formulation

### 2.1 Model of n-DOF teleoperation systems

The dynamics of n-DOF master and slave robots are modeled in the joint space as follows [7]:

$$\begin{aligned} &\boldsymbol{M}_m(\boldsymbol{q}_m)\ddot{\boldsymbol{q}}_m + \boldsymbol{C}_m(\boldsymbol{q}_m,\dot{\boldsymbol{q}}_m)\dot{\boldsymbol{q}}_m + \boldsymbol{G}_m(\boldsymbol{q}_m) + \boldsymbol{d}_m + \boldsymbol{J}_m^{\mathrm{T}}(\boldsymbol{q}_m)\boldsymbol{f}_h = \boldsymbol{\tau}_m,\\ &\boldsymbol{M}_s(\boldsymbol{q}_s)\ddot{\boldsymbol{q}}_s + \boldsymbol{C}_s(\boldsymbol{q}_s,\dot{\boldsymbol{q}}_s)\dot{\boldsymbol{q}}_s + \boldsymbol{G}_s(\boldsymbol{q}_s) + \boldsymbol{d}_s + \boldsymbol{J}_s^{\mathrm{T}}(\boldsymbol{q}_s)\boldsymbol{f}_e = \boldsymbol{\tau}_s, \end{aligned} \tag{1}$$

where the subscripts $m$ and $s$ denote the master and slave robots respectively, $\boldsymbol{q}_m,\ \boldsymbol{q}_s \in \mathbb{R}^{n\times 1}$ are the joint angle positions, $\boldsymbol{M}_m(\boldsymbol{q}_m),\ \boldsymbol{M}_s(\boldsymbol{q}_s) \in \mathbb{R}^{n\times n}$ are the inertia matrices, $\boldsymbol{C}_m(\boldsymbol{q}_m,\dot{\boldsymbol{q}}_m),\ \boldsymbol{C}_s(\boldsymbol{q}_s,\dot{\boldsymbol{q}}_s) \in \mathbb{R}^{n\times n}$ include the Coriolis and centrifugal terms, $\boldsymbol{G}_m(\boldsymbol{q}_m),\ \boldsymbol{G}_s(\boldsymbol{q}_s) \in \mathbb{R}^{n\times 1}$ are the gravity terms, $\boldsymbol{d}_m,\ \boldsymbol{d}_s \in \mathbb{R}^{n\times 1}$ are the external disturbance torques, $\boldsymbol{\tau}_m, \boldsymbol{\tau}_s \in \mathbb{R}^{n\times 1}$ with $1 \leqslant r \leqslant 3$ are the control torques (i.e., the electrical torques of master and slave robots), $\boldsymbol{J}_m(\boldsymbol{q}_m),\ \boldsymbol{J}_s(\boldsymbol{q}_s) \in \mathbb{R}^{n\times r}$ are the Jacobian matrices of the master and slave robots, $\boldsymbol{f}_h,\ \boldsymbol{f}_e \in \mathbb{R}^{r\times 1}$ denote the contact force that the operator applies to the master robot and the environment applies to the slave robot, respectively. The kinematics of the end effector positions of master and slave robots in the task space (Cartesian space) can be obtained as follows:

$$\begin{aligned} &\boldsymbol{x}_m = \boldsymbol{h}_m(\boldsymbol{q}_m),\quad \dot{\boldsymbol{x}}_m = \boldsymbol{J}_m(\boldsymbol{q}_m)\dot{\boldsymbol{q}}_m,\quad \ddot{\boldsymbol{x}}_m = \boldsymbol{J}_m(\boldsymbol{q}_m)\ddot{\boldsymbol{q}}_m + \dot{\boldsymbol{J}}_m(\boldsymbol{q}_m)\dot{\boldsymbol{q}}_m,\\ &\boldsymbol{x}_s = \boldsymbol{h}_s(\boldsymbol{q}_s),\quad \dot{\boldsymbol{x}}_s = \boldsymbol{J}_s(\boldsymbol{q}_s)\dot{\boldsymbol{q}}_s,\quad \ddot{\boldsymbol{x}}_s = \boldsymbol{J}_s(\boldsymbol{q}_s)\ddot{\boldsymbol{q}}_s + \dot{\boldsymbol{J}}_s(\boldsymbol{q}_s)\dot{\boldsymbol{q}}_s, \end{aligned} \tag{2}$$

where $\boldsymbol{x}_m,\ \boldsymbol{x}_s \in \mathbb{R}^{r\times 1}$ are the end effector positions of master and slave robots, $\boldsymbol{h}_m(\cdot),\ \boldsymbol{h}_s(\cdot) \in \mathbb{R}^n \to \mathbb{R}^r$ are nonlinear matrix functions which are used to transfer the robots' positions from joint space to task space. The contact forces $\boldsymbol{f}_h$ and $\boldsymbol{f}_e$ are naturally specified in the task space and they are usually modeled as mass spring damper [11]:

$$\boldsymbol{f}_h = \boldsymbol{f}_h^r - (\boldsymbol{B}_h\dot{\boldsymbol{x}}_m + \boldsymbol{K}_h\boldsymbol{x}_m), \qquad \boldsymbol{f}_e = \boldsymbol{f}_e^r - (\boldsymbol{B}_e\dot{\boldsymbol{x}}_s + \boldsymbol{K}_e\boldsymbol{x}_s), \tag{3}$$

where $\boldsymbol{B}_h = b_h\boldsymbol{I},\ \boldsymbol{K}_h = k_h\boldsymbol{I},\ \boldsymbol{B}_e = b_e\boldsymbol{I},\ \boldsymbol{K}_e = k_e\boldsymbol{I}$, in which $\boldsymbol{I} \in \mathbb{R}^{r\times r}$ is an identity matrix, $b_h, k_h, b_e, k_e$ are positive constants, $\boldsymbol{f}_h^r,\ \boldsymbol{f}_e^r \in \mathbb{R}^{r\times 1}$ are the exogenous forces of the human operator and the environment, respectively.

### 2.2 Control objective analysis

To realize the bilateral haptic transmission between the remote site and the local site, the control objective of the teleoperation systems can be specified as the following two tasks.

(1) Motion reproduction. To transmit the local master robot's motions to the slave robot in the remote site, the positions of master and slave robots should be the same:

$$\boldsymbol{x}_m - \boldsymbol{x}_s \to 0. \tag{4}$$

(2) Force haptic. To haptic the contact force of the slave robot applied by the environment in the remote site, the force from the environment should be transmitted to the operator vividly:

$$\boldsymbol{f}_h + \boldsymbol{f}_e \to 0. \tag{5}$$

To handle more challenging cases such as manipulating heavy loads by amplifying operator's forces or performing dexterous manipulation by reducing motions, the above control tasks are usually transformed as

$$\boldsymbol{x}_m - \boldsymbol{\alpha}\boldsymbol{x}_s \to 0, \quad \boldsymbol{f}_h + \boldsymbol{\beta}\boldsymbol{f}_e \to 0, \tag{6}$$

where $\boldsymbol{\alpha} = \alpha\boldsymbol{I},\ \boldsymbol{\beta} = \beta\boldsymbol{I}$, in which $\boldsymbol{I} \in \mathbb{R}^{r\times r}$ is an identity matrix, and $\alpha$, $\beta$ are positive constants. It is obvious that when $\alpha = \beta = 1$ the control tasks in (6) reduce to the control tasks in (4) and (5).

## 3 Analysis of existing composite bilateral control methods

Before presenting our proposed method, it is necessary to analyse the existing bilateral control methods in a technique depth. The position dynamics of master and slave robots in task space can be obtained from (1) and (2):

$$\boldsymbol{m}_m\ddot{\boldsymbol{x}}_m = \boldsymbol{f}_m - \left[\boldsymbol{J}_m^{\mathrm{T}}(\boldsymbol{q}_m)\right]^{-1}\boldsymbol{\tau}_{dM} + \boldsymbol{m}_m\dot{\boldsymbol{J}}_m(\boldsymbol{q}_m)\dot{\boldsymbol{q}}_m, \quad \boldsymbol{m}_s\ddot{\boldsymbol{x}}_s = \boldsymbol{f}_s - \left[\boldsymbol{J}_s^{\mathrm{T}}(\boldsymbol{q}_s)\right]^{-1}\boldsymbol{\tau}_{dS} + \boldsymbol{m}_s\dot{\boldsymbol{J}}_s(\boldsymbol{q}_s)\dot{\boldsymbol{q}}_s, \tag{7}$$

with

$$\begin{aligned}
&\boldsymbol{m}_m = \left[\boldsymbol{J}_m^{\mathrm{T}}(\boldsymbol{q}_m)\right]^{-1}\boldsymbol{M}_m(\boldsymbol{q}_m)\boldsymbol{J}_m^{-1}(\boldsymbol{q}_m), \quad \boldsymbol{f}_m = \left[\boldsymbol{J}_m^{\mathrm{T}}(\boldsymbol{q}_m)\right]^{-1}\boldsymbol{\tau}_m,\\
&\boldsymbol{\tau}_{dM} = \boldsymbol{J}_m^{\mathrm{T}}(\boldsymbol{q}_m)\boldsymbol{f}_h + \boldsymbol{C}_m(\boldsymbol{q}_m,\dot{\boldsymbol{q}}_m)\dot{\boldsymbol{q}}_m + \boldsymbol{G}_m(\boldsymbol{q}_m) + \boldsymbol{d}_m,\\
&\boldsymbol{m}_s = \left[\boldsymbol{J}_s^{\mathrm{T}}(\boldsymbol{q}_s)\right]^{-1}\boldsymbol{M}_s(\boldsymbol{q}_s)\boldsymbol{J}_s^{-1}(\boldsymbol{q}_s), \quad \boldsymbol{f}_s = \left[\boldsymbol{J}_s^{\mathrm{T}}(\boldsymbol{q}_s)\right]^{-1}\boldsymbol{\tau}_s,\\
&\boldsymbol{\tau}_{dS} = \boldsymbol{J}_s^{\mathrm{T}}(\boldsymbol{q}_s)\boldsymbol{f}_e + \boldsymbol{C}_s(\boldsymbol{q}_s,\dot{\boldsymbol{q}}_s)\dot{\boldsymbol{q}}_s + \boldsymbol{G}_s(\boldsymbol{q}_s) + \boldsymbol{d}_s,
\end{aligned}$$

where $\boldsymbol{f}_m$ and $\boldsymbol{f}_s$ are the virtual force controllers of master and slave robots. According to (7), two well-known existing composite bilateral control methods (as shown in Figure 2) which are designed based on WDOB and MDOB respectively are introduced in the following part. Our motivations are given later to show how their shortcomings can be overcome.

### 3.1 Workspace disturbance observer based method

To employ the LDOB in work space, the nominal model of master and slave robots in work space are chosen based on (7) as the following linear model:

$$\boldsymbol{m}_{mn}\ddot{\boldsymbol{x}}_m = \boldsymbol{f}_m - \boldsymbol{f}_{dm}, \quad \boldsymbol{m}_{sn}\ddot{\boldsymbol{x}}_s = \boldsymbol{f}_s - \boldsymbol{f}_{ds}, \tag{8}$$

with

$$\begin{aligned}
&\boldsymbol{f}_{dm} = \left[\boldsymbol{J}_m^{\mathrm{T}}(\boldsymbol{q}_m)\right]^{-1}\boldsymbol{\tau}_{dM} - \boldsymbol{m}_m\dot{\boldsymbol{J}}_m(\boldsymbol{q}_m)\dot{\boldsymbol{q}}_m + (\boldsymbol{m}_m - \boldsymbol{m}_{mn})\ddot{\boldsymbol{x}}_m,\\
&\boldsymbol{f}_{ds} = \left[\boldsymbol{J}_s^{\mathrm{T}}(\boldsymbol{q}_s)\right]^{-1}\boldsymbol{\tau}_{dS} - \boldsymbol{m}_s\dot{\boldsymbol{J}}_s(\boldsymbol{q}_s)\dot{\boldsymbol{q}}_s + (\boldsymbol{m}_s - \boldsymbol{m}_{sn})\ddot{\boldsymbol{x}}_s,
\end{aligned}$$

where $\boldsymbol{m}_{mn}$, $\boldsymbol{m}_{sn}$ are constant diagonal matrices and they are the nominal values of $\boldsymbol{m}_m$ and $\boldsymbol{m}_s$. The WDOB [11] is designed to estimate the lumped disturbance in (8), given by

$$\widehat{\boldsymbol{f}}_{di} = \boldsymbol{G}_{i1}(s)\left[\boldsymbol{f}_i + \boldsymbol{G}_{i2}(s)\boldsymbol{m}_{in}\dot{\boldsymbol{x}}_i\right] - \boldsymbol{G}_{i2}(s)\boldsymbol{m}_{in}\dot{\boldsymbol{x}}_i, \tag{9}$$

with

$$\boldsymbol{G}_{i1} = \mathrm{diag}\left[\frac{g_i^1}{s+g_i^1},\ldots,\frac{g_i^r}{s+g_i^r}\right], \quad \boldsymbol{G}_{i2} = \mathrm{diag}[g_i^1,\ldots,g_i^r],$$

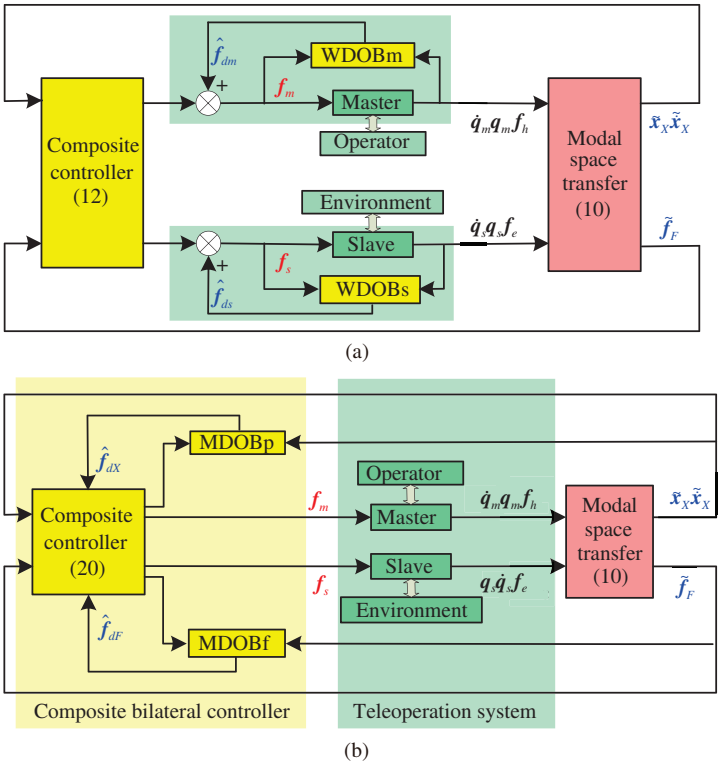


**Figure 2** (Color online) Control structures of two typical existing composite bilateral control methods. (a) WDOB based composite bilateral controller; (b) MDOB based composite bilateral controller.

where $i = m, s$ represent the master and slave robots respectively, $g_i^1, \ldots, g_i^r$ are positive constants. The states in work space can be transformed into the modal space through the following transformation [11]:

$$\widetilde{\boldsymbol{x}} = \begin{bmatrix} \widetilde{\boldsymbol{x}}_X \\ \widetilde{\boldsymbol{x}}_F \end{bmatrix} = \begin{bmatrix} \boldsymbol{I} & -\boldsymbol{\alpha} \\ \boldsymbol{I} & \boldsymbol{\beta} \end{bmatrix} \begin{bmatrix} \boldsymbol{x}_m \\ \boldsymbol{x}_s \end{bmatrix} = \boldsymbol{J}_t \begin{bmatrix} \boldsymbol{x}_m \\ \boldsymbol{x}_s \end{bmatrix}, \quad \widetilde{\boldsymbol{f}} = \begin{bmatrix} \widetilde{\boldsymbol{f}}_X \\ \widetilde{\boldsymbol{f}}_F \end{bmatrix} = \boldsymbol{J}_t \begin{bmatrix} \boldsymbol{f}_h \\ \boldsymbol{f}_e \end{bmatrix}, \tag{10}$$

where $\widetilde{\boldsymbol{x}}$ is the sate vector in modal space and $\boldsymbol{J}_t$ is a constant matrix which is determined by position and force scaling matrices. The dynamics (8) can be transformed into the modal space based on (10) as

$$\widetilde{\boldsymbol{m}}\ddot{\widetilde{\boldsymbol{x}}} = \boldsymbol{J}_t \begin{bmatrix} \boldsymbol{f}_m - \boldsymbol{f}_{dm} \\ \boldsymbol{f}_s - \boldsymbol{f}_{ds} \end{bmatrix}, \tag{11}$$

with

$$\widetilde{\boldsymbol{m}} = \boldsymbol{J}_t \begin{bmatrix} \boldsymbol{m}_{mn} & 0 \\ 0 & \boldsymbol{m}_{sn} \end{bmatrix} \boldsymbol{J}_t^{-1} = \begin{bmatrix} \widetilde{\boldsymbol{m}}_{11} & \widetilde{\boldsymbol{m}}_{12} \\ \widetilde{\boldsymbol{m}}_{21} & \widetilde{\boldsymbol{m}}_{22} \end{bmatrix}.$$

The WDOB based composite bilateral controller is designed based on the above transformation as

$$\begin{bmatrix} \boldsymbol{f}_m \\ \boldsymbol{f}_s \end{bmatrix} = \boldsymbol{J}_t^{-1} \begin{bmatrix} \boldsymbol{M}_1 \boldsymbol{C}_P(s) \widetilde{\boldsymbol{x}}_X + \boldsymbol{M}_2 \widetilde{\boldsymbol{m}}_{22} \boldsymbol{B}_h^{-1} \boldsymbol{C}_F(s) \widetilde{\boldsymbol{f}}_F \\ \widetilde{\boldsymbol{m}}_{22} \boldsymbol{B}_h^{-1} \boldsymbol{C}_F(s) \widetilde{\boldsymbol{f}}_F \end{bmatrix} + \begin{bmatrix} \widehat{\boldsymbol{f}}_{dm} \\ \widehat{\boldsymbol{f}}_{ds} \end{bmatrix}, \tag{12}$$

with

$$\boldsymbol{M}_1 = \widetilde{\boldsymbol{m}}_{11} - \widetilde{\boldsymbol{m}}_{12} \widetilde{\boldsymbol{m}}_{22}^{-1} \widetilde{\boldsymbol{m}}_{21}, \qquad \boldsymbol{M}_2 = \widetilde{\boldsymbol{m}}_{12} \widetilde{\boldsymbol{m}}_{22}^{-1},$$

where $\widehat{\boldsymbol{f}}_{dm}$ and $\widehat{\boldsymbol{f}}_{ds}$ are obtained from the WDOB (9), $\boldsymbol{C}_P(s)$ and $\boldsymbol{C}_F(s)$ are the baseline feedback controller and designed as

$$\boldsymbol{C}_P(s) = -\boldsymbol{K}_{PP} - \boldsymbol{K}_{PD} s, \quad \boldsymbol{C}_F(s) = \boldsymbol{K}_F, \tag{13}$$

where $\boldsymbol{K}_{PP} = k_{PP}\boldsymbol{I}$, $\boldsymbol{K}_{PD} = k_{PD}\boldsymbol{I}$ and $\boldsymbol{K}_F = k_F \boldsymbol{I}$, in which $\boldsymbol{I} \in \mathbb{R}^{r \times r}$ is an identity matrix.

The close-loop dynamics of teleoperation system can be obtained by substituting the MDOB based controller (12) into dynamics (11) as

$$\begin{aligned}\ddot{\widetilde{\boldsymbol{x}}}_X &= -\boldsymbol{K}_{PP}\widetilde{\boldsymbol{x}}_X - \boldsymbol{K}_{PD}\dot{\widetilde{\boldsymbol{x}}}_X + \boldsymbol{M}_1^{-1}\widetilde{\boldsymbol{e}}_1 - \boldsymbol{M}_1^{-1}\boldsymbol{M}_2\widetilde{\boldsymbol{e}}_2,\\ \ddot{\widetilde{\boldsymbol{x}}}_F &= \boldsymbol{B}_h^{-1}\boldsymbol{K}_F\widetilde{\boldsymbol{f}}_F - \widetilde{\boldsymbol{m}}_{22}^{-1}\widetilde{\boldsymbol{m}}_{21}\ddot{\widetilde{\boldsymbol{x}}}_X + \widetilde{\boldsymbol{m}}_{22}^{-1}\widetilde{\boldsymbol{e}}_2,\end{aligned} \tag{14}$$

with

$$\widetilde{\boldsymbol{e}}_1 = \left(\hat{\boldsymbol{f}}_{dm} - \boldsymbol{f}_{dm}\right) - \boldsymbol{\alpha}\left(\hat{\boldsymbol{f}}_{ds} - \boldsymbol{f}_{ds}\right), \quad \widetilde{\boldsymbol{e}}_2 = \left(\hat{\boldsymbol{f}}_{dm} - \boldsymbol{f}_{dm}\right) + \boldsymbol{\beta}\left(\hat{\boldsymbol{f}}_{ds} - \boldsymbol{f}_{ds}\right).$$

With (10) in mind, we can obtain from (3) that

$$-\boldsymbol{B}_h\ddot{\widetilde{\boldsymbol{x}}}_F = \dot{\widetilde{\boldsymbol{f}}}_F - \left(\dot{\boldsymbol{f}}_h^r + \boldsymbol{\beta}\dot{\boldsymbol{f}}_e^r\right) + (\boldsymbol{K}_h\dot{\boldsymbol{x}}_m + \boldsymbol{\beta}\boldsymbol{K}_e\dot{\boldsymbol{x}}_s) + \boldsymbol{\beta}(\boldsymbol{B}_e - \boldsymbol{B}_h)\ddot{\boldsymbol{x}}_s. \tag{15}$$

Combining (14) and (15) yields the close-loop force tracking error dynamics under the WDOB based composite controller (12) as

$$\begin{aligned}\dot{\widetilde{\boldsymbol{f}}}_F =& -\boldsymbol{K}_F\widetilde{\boldsymbol{f}}_F + \boldsymbol{B}_h\widetilde{\boldsymbol{m}}_{\boldsymbol{22}}^{-\boldsymbol{1}}\widetilde{\boldsymbol{m}}_{\boldsymbol{21}}\ddot{\widetilde{\boldsymbol{x}}}_X - \boldsymbol{B}_h\widetilde{\boldsymbol{m}}_{\boldsymbol{22}}^{-\boldsymbol{1}}\widetilde{\boldsymbol{e}}_2 + (\dot{\boldsymbol{f}}_h^r + \boldsymbol{\beta}\dot{\boldsymbol{f}}_e^r)\\ &- \boldsymbol{\beta}\left(\boldsymbol{B}_e - \boldsymbol{B}_h\right)\ddot{\boldsymbol{x}}_s - (\boldsymbol{K}_h\dot{\boldsymbol{x}}_m + \boldsymbol{\beta}\boldsymbol{K}_e\dot{\boldsymbol{x}}_s).\end{aligned} \tag{16}$$

**Remark 1.** Eq. (16) shows that the force tracking error dynamics under this composite controller are coupled with the position tracking error dynamics and system states. The coupling may degrade the steady-state and dynamic performance or even result in unstable control performance of the force tracking error system.

### 3.2 Modal space disturbance observer based method

The MDOB based composite bilateral controller [12] achieves the complete decoupling of position and force tracking error dynamics via designing LDOBs in the modal space. Combining (7) and (10) yields the system dynamics in modal space as

$$\overline{\boldsymbol{m}}(\boldsymbol{q}_m, \boldsymbol{q}_s)\ddot{\widetilde{\boldsymbol{x}}} = \boldsymbol{J}_t \begin{bmatrix} \boldsymbol{f}_m - \left[\boldsymbol{J}_m^{\mathrm{T}}(\boldsymbol{q}_m)\right]^{-1}\boldsymbol{\tau}_{dM} + \boldsymbol{m}_m\dot{\boldsymbol{J}}_m(\boldsymbol{q}_m)\dot{\boldsymbol{q}}_m \\ \boldsymbol{f}_s - \left[\boldsymbol{J}_s^{\mathrm{T}}(\boldsymbol{q}_s)\right]^{-1}\boldsymbol{\tau}_{dS} + \boldsymbol{m}_s\dot{\boldsymbol{J}}_s(\boldsymbol{q}_s)\dot{\boldsymbol{q}}_s \end{bmatrix}, \tag{17}$$

with

$$\overline{\boldsymbol{m}}(\boldsymbol{q}_m, \boldsymbol{q}_s) = \boldsymbol{J}_t \begin{bmatrix} \boldsymbol{m}_m & 0 \\ 0 & \boldsymbol{m}_s \end{bmatrix} \boldsymbol{J}_t^{-1} = \begin{bmatrix} \overline{\boldsymbol{m}}_{11} & \overline{\boldsymbol{m}}_{12} \\ \overline{\boldsymbol{m}}_{21} & \overline{\boldsymbol{m}}_{22} \end{bmatrix}.$$

The nominal model of system states in modal space is designed based on (17) as

$$\begin{bmatrix} \overline{\boldsymbol{m}}_{Xn} & 0 \\ 0 & \overline{\boldsymbol{m}}_{Fn} \end{bmatrix} \begin{bmatrix} \ddot{\widetilde{\boldsymbol{x}}}_X \\ \ddot{\widetilde{\boldsymbol{x}}}_F \end{bmatrix} = \boldsymbol{J}_t \begin{bmatrix} \boldsymbol{f}_m \\ \boldsymbol{f}_s \end{bmatrix} - \begin{bmatrix} \boldsymbol{f}_{dX} \\ \boldsymbol{f}_{dF} \end{bmatrix}, \tag{18}$$

with

$$\begin{bmatrix} \boldsymbol{f}_{dX} \\ \boldsymbol{f}_{dF} \end{bmatrix} = \begin{bmatrix} (\overline{\boldsymbol{m}}_{11} - \overline{\boldsymbol{m}}_{Xn})\ddot{\widetilde{\boldsymbol{x}}}_X + \overline{\boldsymbol{m}}_{12}\ddot{\widetilde{\boldsymbol{x}}}_F \\ (\overline{\boldsymbol{m}}_{22} - \overline{\boldsymbol{m}}_{Fn})\ddot{\widetilde{\boldsymbol{x}}}_F + \overline{\boldsymbol{m}}_{21}\ddot{\widetilde{\boldsymbol{x}}}_X \end{bmatrix} - \boldsymbol{J}_t \begin{bmatrix} -\left[\boldsymbol{J}_m^{\mathrm{T}}(\boldsymbol{q}_m)\right]^{-1}\boldsymbol{\tau}_{dM} + \boldsymbol{m}_m\dot{\boldsymbol{J}}_m(\boldsymbol{q}_m)\dot{\boldsymbol{q}}_m \\ -\left[\boldsymbol{J}_s^{\mathrm{T}}(\boldsymbol{q}_s)\right]^{-1}\boldsymbol{\tau}_{dS} + \boldsymbol{m}_s\dot{\boldsymbol{J}}_s(\boldsymbol{q}_s)\dot{\boldsymbol{q}}_s \end{bmatrix},$$

where $\overline{\boldsymbol{m}}_{Xn}$ and $\overline{\boldsymbol{m}}_{Fn}$ are positive constant diagonal matrices and they are the nominal values of $\overline{\boldsymbol{m}}_{11}$ and $\overline{\boldsymbol{m}}_{22}$. The MDOB [12] is designed based on the linear model (18) as

$$\begin{bmatrix} \hat{\boldsymbol{f}}_{dX} \\ \hat{\boldsymbol{f}}_{dF} \end{bmatrix} = \boldsymbol{G}_1(s)\left(\boldsymbol{J}_t \begin{bmatrix} \boldsymbol{f}_m \\ \boldsymbol{f}_s \end{bmatrix} + \boldsymbol{G}_2(s)\overline{\boldsymbol{m}}_n\dot{\widetilde{\boldsymbol{x}}}\right) - \boldsymbol{G}_2(s)\overline{\boldsymbol{m}}_n\dot{\widetilde{\boldsymbol{x}}}, \tag{19}$$

with

$$\boldsymbol{G}_1(s) = \mathrm{diag}\left[\frac{\bar{g}_1}{s+\bar{g}_1}, \ldots, \frac{\bar{g}_{2r}}{s+\bar{g}_{2r}}\right], \quad \boldsymbol{G}_2(s) = \mathrm{diag}[\bar{g}_1, \ldots, \bar{g}_{2r}],$$

where $\overline{\boldsymbol{m}}_n = \mathrm{diag}[\overline{\boldsymbol{m}}_{Xn}, \overline{\boldsymbol{m}}_{Fn}]$, $\bar{g}_1$, ..., $\bar{g}_{2r}$ are positive constants. The final MDOB based composite bilateral controller [12] is designed based on (18) as

$$\begin{bmatrix} \boldsymbol{f}_m \\ \boldsymbol{f}_s \end{bmatrix} = \boldsymbol{J}_t^{-1} \begin{bmatrix} \overline{\boldsymbol{m}}_{Xn}\boldsymbol{C}_P(s)\widetilde{\boldsymbol{x}}_X + \widehat{\boldsymbol{f}}_{dX} \\ \overline{\boldsymbol{m}}_{Fn}\boldsymbol{B}_h^{-1}\boldsymbol{C}_F(s)\widetilde{\boldsymbol{f}}_F + \widehat{\boldsymbol{f}}_{dF} \end{bmatrix}, \tag{20}$$

where $\widehat{\boldsymbol{f}}_{dX}$ and $\widehat{\boldsymbol{f}}_{dF}$ are obtained from MDOB (19), $\boldsymbol{C}_P(s)$ and $\boldsymbol{C}_F(s)$ are the same with (13).

Substituting the composite bilateral controller (20) into the modal space dynamics (18) yields:

$$\ddot{\widetilde{\boldsymbol{x}}}_X = -\boldsymbol{K}_{PP}\widetilde{\boldsymbol{x}}_X - \boldsymbol{K}_{PD}\dot{\widetilde{\boldsymbol{x}}}_X + \left(\widehat{\boldsymbol{f}}_{dX} - \boldsymbol{f}_{dX}\right), \quad \ddot{\widetilde{\boldsymbol{x}}}_F = \boldsymbol{B}_h^{-1}\boldsymbol{K}_F\widetilde{\boldsymbol{f}}_F + \left(\widehat{\boldsymbol{f}}_{dF} - \boldsymbol{f}_{dF}\right). \tag{21}$$

Combining (15) and (21) yields the close-loop force tracking error dynamics under the composite controller (20) as

$$\dot{\widetilde{\boldsymbol{f}}}_F = -\boldsymbol{K}_F\widetilde{\boldsymbol{f}}_F - \boldsymbol{B}_h\left(\widehat{\boldsymbol{f}}_{dF} - \boldsymbol{f}_{dF}\right) + \left(\dot{\boldsymbol{f}}_h^r + \boldsymbol{\beta}\dot{\boldsymbol{f}}_e^r\right) - \boldsymbol{\beta}(\boldsymbol{B}_e - \boldsymbol{B}_h)\ddot{\boldsymbol{x}}_s - (\boldsymbol{K}_h\dot{\boldsymbol{x}}_m + \boldsymbol{\beta}\boldsymbol{K}_e\dot{\boldsymbol{x}}_s). \tag{22}$$

**Remark 2.** It can be observed from (21) and (22) that the MDOB based composite controller achieves the complete decoupling of force and position tracking error dynamics as desired. While Eq. (22) indicts that the force tracking error cannot be driven to the desired equilibrium point unless the steady-state states of the teleoperation systems are constants.

### 3.3 Analysis and motivation

**Disturbance estimation performance.** The disturbance estimations of WDOB and MDOB in the two methods above can be obtained from (9) and (19) as follows:

$$\widehat{\boldsymbol{f}}_{dm} = \boldsymbol{G}_{m1}(s)\boldsymbol{f}_{dm}, \quad \widehat{\boldsymbol{f}}_{ds} = \boldsymbol{G}_{s1}(s)\boldsymbol{f}_{ds}, \quad \left[\hat{\boldsymbol{f}}_{dX}\ \hat{\boldsymbol{f}}_{dF}\right]^{\mathrm{T}} = \boldsymbol{G}_1(s)[\boldsymbol{f}_{dX}\ \boldsymbol{f}_{dF}]^{\mathrm{T}}. \tag{23}$$

It concludes from (23) that the WDOB and MDOB are mainly effective to the low-frequency disturbances. However, it follows from (8) and (18) that the ignored nonlinear dynamics are considered as a part of disturbances in both the WDOB and MDOB (please refer to the expressions of $\boldsymbol{f}_{dm}$, $\boldsymbol{f}_{ds}$ and $\boldsymbol{f}_{dX}$, $\boldsymbol{f}_{dF}$). Consequently, the estimation performance of WDOB and MDOB degrades significantly when the master or slave robot exhibits strong nonlinearity.

**Force tracking performance.** As shown by (16) and (22), the force tracking error dynamics under the WDOB and MDOB based composite bilateral controllers are influenced by system states. Both of the above controllers alleviate the influences through a passive way, where a controller cannot react directly and fast enough, although it can finally suppress the influences through feedback regulation in a relatively slow way [21].

**Motivation of the work.** To eliminate the influences of nonlinear dynamics and solve the coupling problem between force tracking error dynamics with system states in n-DOF teleoperation systems, we develop a new control framework through the following two steps: (1) Designing a baseline NFL controller based on the nonlinear dynamics in position and force tracking error subsystems such that the position and force tracking error dynamics decouple from system states. (2) Constructing a nonlinear composite bilateral control framework via introducing the disturbance estimations of NDOB into the baseline NFL controller to achieve fast disturbance rejection performance via a feedforward compensation way.

## 4 Nonlinear composite bilateral control framework design and analysis

### 4.1 Baseline nonlinear controller design

Let us define the position tracking error $\boldsymbol{e}_P$ and the force tracking error $\boldsymbol{e}_F$ based on (6) as follows:

$$\boldsymbol{e}_P = \boldsymbol{x}_m - \boldsymbol{\alpha}\boldsymbol{x}_s, \quad \boldsymbol{e}_F = \boldsymbol{f}_h + \boldsymbol{\beta}\boldsymbol{f}_e. \tag{24}$$

The position tracking error dynamics in joint space can be obtained from (1) and (2) as

$$\dot{\boldsymbol{e}}_P = \boldsymbol{J}_m(\boldsymbol{q}_m)\dot{\boldsymbol{q}}_m - \boldsymbol{\alpha}\boldsymbol{J}_s(\boldsymbol{q}_s)\dot{\boldsymbol{q}}_s, \quad \ddot{\boldsymbol{e}}_P = \boldsymbol{u}_P + \boldsymbol{F}_P + \boldsymbol{d}_1, \tag{25}$$

with

$$\begin{aligned}
\boldsymbol{u}_P &= \boldsymbol{J}_m(\boldsymbol{q}_m)\boldsymbol{M}_m^{-1}(\boldsymbol{q}_m)\boldsymbol{\tau}_m - \boldsymbol{\alpha}\boldsymbol{J}_s(\boldsymbol{q}_s)\boldsymbol{M}_s^{-1}(\boldsymbol{q}_s)\boldsymbol{\tau}_s,\\
\boldsymbol{F}_P &= -\boldsymbol{J}_m(\boldsymbol{q}_m)\boldsymbol{M}_m^{-1}(\boldsymbol{q}_m)\left[\boldsymbol{J}_m^{\mathrm{T}}(\boldsymbol{q}_m)\boldsymbol{f}_h + \boldsymbol{C}_m(\boldsymbol{q}_m,\dot{\boldsymbol{q}}_m)\dot{\boldsymbol{q}}_m + \boldsymbol{G}_m(\boldsymbol{q}_m)\right] + \dot{\boldsymbol{J}}_m(\boldsymbol{q}_m)\dot{\boldsymbol{q}}_m\\
&\quad + \boldsymbol{\alpha}\boldsymbol{J}_s(\boldsymbol{q}_s)\boldsymbol{M}_s^{-1}(\boldsymbol{q}_s)\left[\boldsymbol{J}_s^{\mathrm{T}}(\boldsymbol{q}_s)\boldsymbol{f}_e + \boldsymbol{C}_s(\boldsymbol{q}_s,\dot{\boldsymbol{q}}_s)\dot{\boldsymbol{q}}_s + \boldsymbol{G}_s(\boldsymbol{q}_s)\right] - \boldsymbol{\alpha}\dot{\boldsymbol{J}}_s(\boldsymbol{q}_s)\dot{\boldsymbol{q}}_s,\\
\boldsymbol{d}_1(t) &= -\boldsymbol{J}_m(\boldsymbol{q}_m)\boldsymbol{M}_m^{-1}(\boldsymbol{q}_m)\boldsymbol{d}_m + \boldsymbol{\alpha}\boldsymbol{J}_s(\boldsymbol{q}_s)\boldsymbol{M}_s^{-1}(\boldsymbol{q}_s)\boldsymbol{d}_s,
\end{aligned}$$

where $\boldsymbol{u}_P$ is the virtual control action for position control task and $\boldsymbol{d}_1(t)$ is the lumped disturbance in the position control channel. With (24) in mind, the force tracking error dynamics in joint space can be obtained from (1)–(3) as

$$\dot{\boldsymbol{e}}_F = \boldsymbol{u}_F + \boldsymbol{F}_F + \boldsymbol{d}_2(t), \tag{26}$$

with

$$\begin{aligned}
\boldsymbol{u}_F &= -\boldsymbol{B}_h\boldsymbol{J}_m(\boldsymbol{q}_m)\boldsymbol{M}_m^{-1}(\boldsymbol{q}_m)\boldsymbol{\tau}_m - \boldsymbol{\beta}\boldsymbol{B}_e\boldsymbol{J}_s(\boldsymbol{q}_s)\boldsymbol{M}_s^{-1}(\boldsymbol{q}_s)\boldsymbol{\tau}_s,\\
\boldsymbol{F}_F &= \boldsymbol{B}_h\boldsymbol{J}_m(\boldsymbol{q}_m)\boldsymbol{M}_m^{-1}(\boldsymbol{q}_m)\left[\boldsymbol{J}_m^{\mathrm{T}}(\boldsymbol{q}_m)\boldsymbol{f}_h + \boldsymbol{C}_m(\boldsymbol{q}_m,\dot{\boldsymbol{q}}_m)\dot{\boldsymbol{q}}_m + \boldsymbol{G}_m(\boldsymbol{q}_m)\right] - \boldsymbol{B}_h\dot{\boldsymbol{J}}_m(\boldsymbol{q}_m)\dot{\boldsymbol{q}}_m\\
&\quad + \boldsymbol{\beta}\boldsymbol{B}_e\boldsymbol{J}_s(\boldsymbol{q}_s)\boldsymbol{M}_s^{-1}(\boldsymbol{q}_s)\left[\boldsymbol{J}_s^{\mathrm{T}}(\boldsymbol{q}_s)\boldsymbol{f}_e + \boldsymbol{C}_s(\boldsymbol{q}_s,\dot{\boldsymbol{q}}_s)\dot{\boldsymbol{q}}_s + \boldsymbol{G}_s(\boldsymbol{q}_s)\right] - \boldsymbol{\beta}\boldsymbol{B}_e\dot{\boldsymbol{J}}_s(\boldsymbol{q}_s)\dot{\boldsymbol{q}}_s\\
&\quad + \dot{\boldsymbol{f}}_h^r + \boldsymbol{\beta}\dot{\boldsymbol{f}}_e^r - \boldsymbol{K}_h\boldsymbol{J}_m(\boldsymbol{q}_m)\dot{\boldsymbol{q}}_m - \boldsymbol{\beta}\boldsymbol{K}_e\boldsymbol{J}_s(\boldsymbol{q}_s)\dot{\boldsymbol{q}}_s,\\
\boldsymbol{d}_2(t) &= \boldsymbol{B}_h\boldsymbol{J}_m(\boldsymbol{q}_m)\boldsymbol{M}_m^{-1}(\boldsymbol{q}_m)\boldsymbol{d}_m + \boldsymbol{\beta}\boldsymbol{B}_e\boldsymbol{J}_s(\boldsymbol{q}_s)\boldsymbol{M}_s^{-1}(\boldsymbol{q}_s)\boldsymbol{d}_s,
\end{aligned}$$

where $\boldsymbol{u}_F$ is the virtual control action for force control task and $\boldsymbol{d}_2(t)$ is the lumped disturbance in the force control channel. The real control actions $\boldsymbol{\tau}_m$ and $\boldsymbol{\tau}_s$ can be calculated from the virtual control actions $\boldsymbol{u}_P$ and $\boldsymbol{u}_F$ as follows:

$$\begin{aligned}
\boldsymbol{\tau}_m &= -\boldsymbol{M}_m(\boldsymbol{q}_m)\boldsymbol{J}_m^{-1}(\boldsymbol{q}_m)\left(\boldsymbol{\beta}\boldsymbol{B}_e + \boldsymbol{\alpha}\boldsymbol{B}_h\right)^{-1}\left(\boldsymbol{\alpha}\boldsymbol{u}_F - \boldsymbol{\beta}\boldsymbol{B}_e\boldsymbol{u}_P\right),\\
\boldsymbol{\tau}_s &= -\boldsymbol{M}_s(\boldsymbol{q}_s)\boldsymbol{J}_s^{-1}(\boldsymbol{q}_s)\left(\boldsymbol{\beta}\boldsymbol{B}_e + \boldsymbol{\alpha}\boldsymbol{B}_h\right)^{-1}\left(\boldsymbol{B}_h\boldsymbol{u}_P + \boldsymbol{u}_F\right).
\end{aligned} \tag{27}$$

Therefore, the design of bilateral controllers $\boldsymbol{\tau}_m$ and $\boldsymbol{\tau}_s$ in joint space can be transformed to the design of the virtual controllers $\boldsymbol{u}_P$ and $\boldsymbol{u}_F$ in the position and force tracking error subsystems.

The baseline NFL controller can be designed based on (25) and (26) as

$$\boldsymbol{u}_{P0} = -\boldsymbol{F}_P - \boldsymbol{K}_{PD}\dot{\boldsymbol{e}}_P - \boldsymbol{K}_{PP}\boldsymbol{e}_P, \quad \boldsymbol{u}_{F0} = -\boldsymbol{F}_F - \boldsymbol{K}_F\boldsymbol{e}_F, \tag{28}$$

where $\boldsymbol{K}_{PD} = k_{PD}\boldsymbol{I}$, $\boldsymbol{K}_{PP} = k_{PP}\boldsymbol{I}$ and $\boldsymbol{K}_F = k_F\boldsymbol{I}$, in which $\boldsymbol{I} \in \mathbb{R}^{r\times r}$ is an identity matrix, are the controller parameters to be designed. The real control actions under the baseline controller can be obtained by replacing the virtual controllers $\boldsymbol{u}_P$ and $\boldsymbol{u}_F$ in (27) with $\boldsymbol{u}_{P0}$ and $\boldsymbol{u}_{F0}$ in (28).

### 4.2 Nonlinear disturbance observer design

**Assumption 1.** The derivatives of the external disturbance torques $\boldsymbol{d}_m$ and $\boldsymbol{d}_s$ in teleoperation system (1) are bounded, i.e., $||\dot{\boldsymbol{d}}_m||_2 \leqslant k_{dm}$ and $||\dot{\boldsymbol{d}}_s||_2 \leqslant k_{ds}$, where $k_{dm}$ and $k_{ds}$ are two positive constants.

**Assumption 2.** The external disturbance torques $\boldsymbol{d}_m$ and $\boldsymbol{d}_s$ in teleoperation system (1) are constants in their steady states, i.e., $\lim_{t\to\infty}\dot{\boldsymbol{d}}_m = \boldsymbol{0}$ and $\lim_{t\to\infty}\dot{\boldsymbol{d}}_s = \boldsymbol{0}$.

Since $\boldsymbol{M}_m(\boldsymbol{q}_m)$ and $\boldsymbol{M}_s(\boldsymbol{q}_s)$ are the inertial matrices, they are positive definite matrices and invertible. Therefore, the dynamics of teleoperation system (1) can be rewritten as the following form:

$$\begin{bmatrix}\dot{\boldsymbol{q}}_m\\ \ddot{\boldsymbol{q}}_m\end{bmatrix} = \begin{bmatrix}\boldsymbol{0}\\ \boldsymbol{g}_{mu}\end{bmatrix}\boldsymbol{\tau}_m + \begin{bmatrix}\dot{\boldsymbol{q}}_m\\ \boldsymbol{F}_{mn}\end{bmatrix} + \begin{bmatrix}\boldsymbol{0}\\ \boldsymbol{g}_{md}\end{bmatrix}\boldsymbol{d}_m, \quad \begin{bmatrix}\dot{\boldsymbol{q}}_s\\ \ddot{\boldsymbol{q}}_s\end{bmatrix} = \begin{bmatrix}\boldsymbol{0}\\ \boldsymbol{g}_{su}\end{bmatrix}\boldsymbol{\tau}_s + \begin{bmatrix}\dot{\boldsymbol{q}}_s\\ \boldsymbol{F}_{sn}\end{bmatrix} + \begin{bmatrix}\boldsymbol{0}\\ \boldsymbol{g}_{sd}\end{bmatrix}\boldsymbol{d}_s, \tag{29}$$

with

$$\begin{aligned}
&\boldsymbol{g}_{mu} = \boldsymbol{M}_m^{-1}(\boldsymbol{q}_m), \quad \boldsymbol{F}_{mn} = -\boldsymbol{M}_m^{-1}(\boldsymbol{q}_m)\left[\boldsymbol{C}_m(\boldsymbol{q}_m,\dot{\boldsymbol{q}}_m)\dot{\boldsymbol{q}}_m + \boldsymbol{G}_m(\boldsymbol{q}_m) + \boldsymbol{J}_m^{\mathrm{T}}(\boldsymbol{q}_m)\boldsymbol{f}_h\right], \quad \boldsymbol{g}_{md} = -\boldsymbol{M}_m^{-1}(\boldsymbol{q}_m),\\
&\boldsymbol{g}_{su} = \boldsymbol{M}_s^{-1}(\boldsymbol{q}_s), \quad \boldsymbol{F}_{sn} = -\boldsymbol{M}_s^{-1}(\boldsymbol{q}_s)\left[\boldsymbol{C}_s(\boldsymbol{q}_s,\dot{\boldsymbol{q}}_s)\dot{\boldsymbol{q}}_s + \boldsymbol{G}_s(\boldsymbol{q}_s) + \boldsymbol{J}_s^{\mathrm{T}}(\boldsymbol{q}_s)\boldsymbol{f}_e\right], \quad \boldsymbol{g}_{sd} = -\boldsymbol{M}_s^{-1}(\boldsymbol{q}_s).
\end{aligned}$$

The NDOB [14] is introduced and designed to estimate the external disturbances $d_m$ and $d_s$ acting on the master and slave robots in (29) as follows:

$$\text{NDOB1}: \begin{cases} \dot{\boldsymbol{z}}_1 = -\boldsymbol{L}_m \begin{bmatrix} \dot{\boldsymbol{q}}_m \\ \boldsymbol{g}_{md}(\boldsymbol{p}_m + \boldsymbol{z}_1) + \boldsymbol{g}_{mu}\boldsymbol{\tau}_m + \boldsymbol{F}_{mn} \end{bmatrix}, \\ \hat{\boldsymbol{d}}_m = \boldsymbol{z}_1 + \boldsymbol{p}_m, \end{cases}$$

$$\text{NDOB2}: \begin{cases} \dot{\boldsymbol{z}}_2 = -\boldsymbol{L}_s \begin{bmatrix} \dot{\boldsymbol{q}}_s \\ \boldsymbol{g}_{sd}(\boldsymbol{p}_s + \boldsymbol{z}_2) + \boldsymbol{g}_{su}\boldsymbol{\tau}_s + \boldsymbol{F}_{sn} \end{bmatrix}, \\ \hat{\boldsymbol{d}}_s = \boldsymbol{z}_2 + \boldsymbol{p}_s, \end{cases} \tag{30}$$

with

$$\boldsymbol{p}_m = -\boldsymbol{L}_{mc}\boldsymbol{M}_m(\boldsymbol{q}_m)\dot{\boldsymbol{q}}_m, \quad \boldsymbol{L}_m = \begin{bmatrix} \dfrac{\partial \boldsymbol{p}_m}{\partial \boldsymbol{q}_m} & \dfrac{\partial \boldsymbol{p}_m}{\partial \dot{\boldsymbol{q}}_m} \end{bmatrix}, \quad \boldsymbol{p}_s = -\boldsymbol{L}_{sc}\boldsymbol{M}_s(\boldsymbol{q}_s)\dot{\boldsymbol{q}}_s, \quad \boldsymbol{L}_s = \begin{bmatrix} \dfrac{\partial \boldsymbol{p}_s}{\partial \boldsymbol{q}_s} & \dfrac{\partial \boldsymbol{p}_s}{\partial \dot{\boldsymbol{q}}_s} \end{bmatrix},$$

where $\boldsymbol{z}_1 = [z_{11}, \ldots, z_{1n}]^{\mathrm{T}}$, $\boldsymbol{z}_2 = [z_{21}, \ldots, z_{2n}]^{\mathrm{T}}$ are the internal states of observers, $\boldsymbol{L}_{mc} = \mathrm{diag}[l_{11}, \ldots, l_{1n}]$ and $\boldsymbol{L}_{sc} = \mathrm{diag}[l_{21}, \ldots, l_{2n}]$ are constant matrices, $l_{11}, \ldots, l_{1n}$ and $l_{21}, \ldots, l_{2n}$ are the observer gains to be designed, $\hat{\boldsymbol{d}}_m$ and $\hat{\boldsymbol{d}}_s$ are the estimations of disturbances.

**Theorem 1.** Suppose that Assumption 1 is satisfied for the teleoperation system (1). The NDOBs (30) guarantee the disturbance estimation errors converge to a bounded region if the observer gains in (30) are designed as positive constants.

*Proof.* Define the disturbance estimation errors as

$$\boldsymbol{e}_{dm} = \hat{\boldsymbol{d}}_m - \boldsymbol{d}_m, \quad \boldsymbol{e}_{ds} = \hat{\boldsymbol{d}}_s - \boldsymbol{d}_s. \tag{31}$$

Combining (29) and (30) yields the dynamics of estimation errors:

$$\dot{\boldsymbol{e}}_{dm} = -\boldsymbol{L}_{mc}\boldsymbol{e}_{dm} - \dot{\boldsymbol{d}}_m, \qquad \dot{\boldsymbol{e}}_{ds} = -\boldsymbol{L}_{sc}\boldsymbol{e}_{ds} - \dot{\boldsymbol{d}}_s. \tag{32}$$

It is observed from (32) that the disturbance estimation errors $\boldsymbol{e}_{dm}$ and $\boldsymbol{e}_{ds}$ have similarly dynamics. Hence, only the dynamics of $\boldsymbol{e}_{dm}$ is considered in the following part to save space. Since the observer gains in (30) are designed as positive constants, the minimum eigenvalue $\lambda_{\min}(\boldsymbol{L}_{mc})$ of the diagonal matrix $\boldsymbol{L}_{mc}$ is a positive constant. Let us define a Lyapunov function in terms of $\boldsymbol{e}_{dm}$ as

$$V_{dm} = \boldsymbol{e}_{dm}^{\mathrm{T}}\boldsymbol{e}_{dm}. \tag{33}$$

Taking the derivative of $V_{dm}$ along dynamics (32) yields:

$$\dot{V}_{dm} = -2\boldsymbol{e}_{dm}^{\mathrm{T}}\boldsymbol{L}_{mc}\boldsymbol{e}_{dm} - 2\dot{\boldsymbol{d}}_m^{\mathrm{T}}\boldsymbol{e}_{dm} \leqslant -2\lambda_{\min}(\boldsymbol{L}_{mc})||\boldsymbol{e}_{dm}||_2^2 + 2||\dot{\boldsymbol{d}}_m||_2 \cdot ||\boldsymbol{e}_{dm}||_2. \tag{34}$$

With Assumption 1 in mind, it obtains from (34) that

$$\dot{V}_{dm} \leqslant -2\left[\lambda_{\min}(\boldsymbol{L}_{mc})||\boldsymbol{e}_{dm}||_2 - k_{dm}\right] \cdot ||\boldsymbol{e}_{dm}||_2 = -2\left[\lambda_{\min}(\boldsymbol{L}_{mc})||\boldsymbol{e}_{dm}||_2 - k_{dm}\right] V_{dm}^{1/2}. \tag{35}$$

It yields from (35) that $\boldsymbol{e}_{dm}$ converges asymptotically until $||\boldsymbol{e}_{dm}||_2 > \frac{k_{dm}}{\lambda_{\min}(\boldsymbol{L}_{mc})}$ is not satisfied, i.e., the disturbance estimation error converges to the bounded region:

$$||\boldsymbol{e}_{dm}||_2 \leqslant \frac{k_{dm}}{\lambda_{\min}(\boldsymbol{L}_{mc})}. \tag{36}$$

Therefore, the disturbance estimation errors $\boldsymbol{e}_{dm}$ converges to a bounded region. Similar with the above proof, it can be proved that $\boldsymbol{e}_{ds}$ also converges to a bounded region, which completes the proof.

**Theorem 2.** Suppose that Assumptions 1 and 2 are satisfied for teleoperation system (1). The disturbance estimations $\hat{\boldsymbol{d}}_m$ and $\hat{\boldsymbol{d}}_s$ of NDOBs (30) converge to their real values $\boldsymbol{d}_m$ and $\boldsymbol{d}_s$ asymptotically if the observer gains in (30) are designed as positive constants.

*Proof.* Since the observer gains in (30) are designed as positive constants, $-\boldsymbol{L}_{mc}$ is Hurwitz matrix and the dynamics $\dot{\boldsymbol{e}}_{dm} = -\boldsymbol{L}_{mc}\boldsymbol{e}_{dm}$ is asymptotically stable. With Assumption 2 in mind, it derives from the input-to-state stable (ISS) definition in [22] that $\boldsymbol{e}_{dm}$ converge to zero asymptotically. Similarly, it can be proved that $\boldsymbol{e}_{ds}$ converge to zero asymptotically. Therefore, the disturbance estimations $\hat{\boldsymbol{d}}_m$ and $\hat{\boldsymbol{d}}_s$ converge to their real values $\boldsymbol{d}_m$ and $\boldsymbol{d}_s$ asymptotically, which completes the proof.

**Remark 3.** The NDOBs in (30) are employed to estimate the external disturbances $\boldsymbol{d}_m$ and $\boldsymbol{d}_s$, and then the estimations of the induced disturbances $\boldsymbol{d}_1$ and $\boldsymbol{d}_2$ are constructed based on (25) and (26) by combining the information of system states and external disturbances' estimations. This not only improves the estimation precision of induced disturbances, but also relaxes the assumptions on disturbances by separating the external disturbances from the induced disturbances.

### 4.3 Nonlinear composite bilateral control framework design

The lumped disturbances in position and force tracking error subsystems (25) and (26) can be estimated through the estimations of external disturbance torques as

$$\hat{\boldsymbol{d}}_1(t) = -\boldsymbol{f}_1\hat{\boldsymbol{d}}_m + \boldsymbol{\alpha}\boldsymbol{f}_2\hat{\boldsymbol{d}}_s, \qquad \hat{\boldsymbol{d}}_2(t) = \boldsymbol{B}_h\boldsymbol{f}_1\hat{\boldsymbol{d}}_m + \boldsymbol{\beta}\boldsymbol{B}_e\boldsymbol{f}_2\hat{\boldsymbol{d}}_s, \tag{37}$$

with

$$\boldsymbol{f}_1 = \boldsymbol{J}_m(\boldsymbol{q}_m)\boldsymbol{M}_m^{-1}(\boldsymbol{q}_m), \qquad \boldsymbol{f}_2 = \boldsymbol{J}_s(\boldsymbol{q}_s)\boldsymbol{M}_s^{-1}(\boldsymbol{q}_s).$$

The proposed nonlinear composite bilateral controller is designed by introducing the disturbance estimations into the baseline NFL controller (28) as follows

$$\boldsymbol{u}_P = -\boldsymbol{F}_P - \boldsymbol{K}_{PD}\dot{\boldsymbol{e}}_P - \boldsymbol{K}_{PP}\boldsymbol{e}_P - \hat{\boldsymbol{d}}_1, \quad \boldsymbol{u}_F = -\boldsymbol{F}_F - \boldsymbol{K}_F\boldsymbol{e}_F - \hat{\boldsymbol{d}}_2. \tag{38}$$

**Theorem 3.** Suppose that Assumption 1 is satisfied for the teleoperation system (1). The proposed nonlinear composite bilateral controller (38) guarantees the position and force tracking errors converge to a bounded region if the controller parameters are designed as $k_{PP} > 0$, $k_{PD} > 0$, $k_F > 0$ and the observer gains in (30) are designed as positive constants.

*Proof.* With (31) and (37) in mind, substituting the proposed nonlinear composite bilateral controller (38) into the position and force tracking error subsystems (25) and (26) yields:

$$\ddot{\boldsymbol{e}}_P = -\boldsymbol{K}_{PD}\dot{\boldsymbol{e}}_P - \boldsymbol{K}_{PP}\boldsymbol{e}_P + \boldsymbol{f}_1\boldsymbol{e}_{dm} - \boldsymbol{\alpha}\boldsymbol{f}_2\boldsymbol{e}_{ds}, \qquad \dot{\boldsymbol{e}}_F = -\boldsymbol{K}_F\boldsymbol{e}_F - \boldsymbol{B}_h\boldsymbol{f}_1\boldsymbol{e}_{dm} - \boldsymbol{\beta}\boldsymbol{B}_e\boldsymbol{f}_2\boldsymbol{e}_{ds}. \tag{39}$$

Let us introduce new states $\boldsymbol{w}_1 = [\boldsymbol{e}_P \ \dot{\boldsymbol{e}}_P \ \boldsymbol{e}_F]^{\mathrm{T}}$ and $\boldsymbol{w}_2 = [\boldsymbol{e}_{dm} \ \boldsymbol{e}_{ds}]^{\mathrm{T}}$. Combining (32) and (39) yields the close-loop dynamics of system (1) under controller (38) as follows:

$$\dot{\boldsymbol{w}}_1 = \boldsymbol{A}_c\boldsymbol{w}_1 + \boldsymbol{F}_x(\boldsymbol{w}_1)\boldsymbol{w}_2, \tag{40}$$

$$\dot{\boldsymbol{w}}_2 = \boldsymbol{A}_o\boldsymbol{w}_2 + \boldsymbol{D}(t), \tag{41}$$

with

$$\boldsymbol{A}_c = \begin{bmatrix} \boldsymbol{0} & \boldsymbol{I} & \boldsymbol{0} \\ -\boldsymbol{K}_{PP} & -\boldsymbol{K}_{PD} & \boldsymbol{0} \\ \boldsymbol{0} & \boldsymbol{0} & -\boldsymbol{K}_F \end{bmatrix}, \quad \boldsymbol{F}_x(\boldsymbol{w}_1) = \begin{bmatrix} \boldsymbol{0} & \boldsymbol{0} \\ \boldsymbol{f}_1 & -\boldsymbol{\alpha}\boldsymbol{f}_2 \\ -\boldsymbol{B}_h\boldsymbol{f}_1 & -\boldsymbol{\beta}\boldsymbol{B}_e\boldsymbol{f}_2 \end{bmatrix},$$

$$\boldsymbol{A}_o = \begin{bmatrix} -\boldsymbol{L}_{mc} & \boldsymbol{0} \\ \boldsymbol{0} & -\boldsymbol{L}_{sc} \end{bmatrix}, \quad \boldsymbol{D}(t) = \begin{bmatrix} -\dot{\boldsymbol{d}}_m \\ -\dot{\boldsymbol{d}}_s \end{bmatrix}.$$

Since the observer gains in (30) are designed as positive constants and controller parameters are designed as $k_{PP} > 0$, $k_{PD} > 0$, $k_F > 0$, it can be verified that $\boldsymbol{A}_o$ and $\boldsymbol{A}_c$ are Hurwitz matrices. Hence there exist positive definite constant matrices $\boldsymbol{P}_c$, $\boldsymbol{Q}_c$ and $\boldsymbol{P}_o$, $\boldsymbol{Q}_o$ which satisfy

$$\boldsymbol{A}_c^{\mathrm{T}}\boldsymbol{P}_c + \boldsymbol{P}_c\boldsymbol{A}_c = -\boldsymbol{Q}_c, \quad \boldsymbol{A}_o^{\mathrm{T}}\boldsymbol{P}_o + \boldsymbol{P}_o\boldsymbol{A}_o = -\boldsymbol{Q}_o. \tag{42}$$

Let us choose a Lyapunov function in terms of $\boldsymbol{w}_1$ and $\boldsymbol{w}_2$ as

$$V = \boldsymbol{w}_1^{\mathrm{T}}\boldsymbol{P}_c\boldsymbol{w}_1 + \epsilon\boldsymbol{w}_2^{\mathrm{T}}\boldsymbol{P}_o\boldsymbol{w}_2, \tag{43}$$

where $\epsilon$ is a positive constant. With (42) in mind, taking the derivative of $V$ along (40) and (41) yields:

$$\dot{V} = -\boldsymbol{w}_1^{\mathrm{T}}\boldsymbol{Q}_c\boldsymbol{w}_1 - \epsilon\boldsymbol{w}_2^{\mathrm{T}}\boldsymbol{Q}_o\boldsymbol{w}_2 + 2\boldsymbol{w}_1^{\mathrm{T}}\boldsymbol{P}_c\boldsymbol{F}_x(\boldsymbol{w}_1)\boldsymbol{w}_2 + 2\epsilon\boldsymbol{w}_2^{\mathrm{T}}\boldsymbol{P}_o\boldsymbol{D}(t). \tag{44}$$

Since $\boldsymbol{Q}_c$ and $\boldsymbol{Q}_o$ are positive definite constant matrices, it can be verified that

$$\lambda_{Qc1}||\boldsymbol{w}_1||_2^2 \leqslant \boldsymbol{w}_1^{\mathrm{T}}\boldsymbol{Q}_c\boldsymbol{w}_1 \leqslant \lambda_{Qc2}||\boldsymbol{w}_1||_2^2, \qquad \lambda_{Qo1}||\boldsymbol{w}_2||_2^2 \leqslant \boldsymbol{w}_2^{\mathrm{T}}\boldsymbol{Q}_o\boldsymbol{w}_2 \leqslant \lambda_{Qo2}||\boldsymbol{w}_2||_2^2, \tag{45}$$

where $\lambda_{Qc1}$, $\lambda_{Qc2}$ and $\lambda_{Qo1}$, $\lambda_{Qo2}$ are the minimum and maximum eigenvalues of $\boldsymbol{Q}_c$ and $\boldsymbol{Q}_o$ respectively. Combining (44) and (45) yields:

$$\begin{aligned}\dot{V} &\leqslant -\lambda_{Qc1}||\boldsymbol{w}_1||_2^2 - \epsilon\lambda_{Qo1}||\boldsymbol{w}_2||_2^2 + 2\boldsymbol{w}_1^{\mathrm{T}}\boldsymbol{P}_c\boldsymbol{F}_x(\boldsymbol{w}_1)\boldsymbol{w}_2 + 2\epsilon\boldsymbol{w}_2^{\mathrm{T}}\boldsymbol{P}_o\boldsymbol{D}(t)\\ &\leqslant -\lambda_{Qc1}||\boldsymbol{w}_1||_2^2 - \epsilon\lambda_{Qo1}||\boldsymbol{w}_2||_2^2 + 2\lambda_{Pc2}||\boldsymbol{w}_1||_2 \cdot ||\boldsymbol{F}_x(\boldsymbol{w}_1)\boldsymbol{w}_2||_2 + 2\epsilon\lambda_{Po2}||\boldsymbol{w}_2||_2 \cdot ||\boldsymbol{D}(t)||_2,\end{aligned} \tag{46}$$

where $\lambda_{Pc2}$ and $\lambda_{Po2}$ are the maximum eigenvalues of $\boldsymbol{P}_c$ and $\boldsymbol{P}_o$ respectively.

Since $\boldsymbol{M}_m(\boldsymbol{q}_m)$ is the inertial matrix of master robot, it is positive definite and its eigenvalues are positive. Therefore, the maximum eigenvalue of $\boldsymbol{M}_m^{-1}(\boldsymbol{q}_m)$ is bounded. $\boldsymbol{J}_m(\boldsymbol{q}_m)$ is the Jacobian matrix of the master robot and it is the scaling function from joint speed to the position speed, hence all the elements in $\boldsymbol{J}_m(\boldsymbol{q}_m)$ are bounded and its maximum eigenvalue $\lambda_{Jm}$ is bounded. Therefore, the maximum eigenvalue of $\boldsymbol{f}_1$ in (37) is bounded. Similar with the above statements, we can obtain that the maximum eigenvalue of $\boldsymbol{f}_2$ is bounded. Considering $\boldsymbol{\alpha}$, $\boldsymbol{\beta}$, $\boldsymbol{B}_e$ and $\boldsymbol{B}_h$ are constant matrices, we can conclude from the expression of $\boldsymbol{F}_x(\boldsymbol{w}_1)$ in (40) that the maximum eigenvalue of $\boldsymbol{F}_x(\boldsymbol{w}_1)^{\mathrm{T}} \cdot \boldsymbol{F}_x(\boldsymbol{w}_1)$ is bounded. Let $\lambda_{Fx2}$ denote the upper bound of the eigenvalue of $\boldsymbol{F}_x(\boldsymbol{w}_1)^{\mathrm{T}} \cdot \boldsymbol{F}_x(\boldsymbol{w}_1)$. We have

$$||\boldsymbol{F}_x(\boldsymbol{w}_1)\boldsymbol{w}_2||_2 = ||\boldsymbol{w}_2^{\mathrm{T}}\boldsymbol{F}_x(\boldsymbol{w}_1)^{\mathrm{T}}\boldsymbol{F}_x(\boldsymbol{w}_1)\boldsymbol{w}_2||_2^{1/2} \leqslant \sqrt{\lambda_{Fx2}}||\boldsymbol{w}_2||_2. \tag{47}$$

Substituting (47) into (46) obtains

$$\begin{aligned}\dot{V} &\leqslant -\lambda_{Qc1}||\boldsymbol{w}_1||_2^2 - \epsilon\lambda_{Qo1}||\boldsymbol{w}_2||_2^2 + 2\sqrt{\frac{\lambda_{Qc1}}{2}}||\boldsymbol{w}_1||_2 \cdot \sqrt{\frac{2\lambda_{Fx2}}{\lambda_{Qc1}}}\lambda_{Pc2}||\boldsymbol{w}_2||_2\\ &\quad + 2\sqrt{\frac{\epsilon\lambda_{Qo1}}{2}}||\boldsymbol{w}_2||_2 \cdot \sqrt{\frac{2\epsilon}{\lambda_{Qo1}}}\lambda_{Po2}||\boldsymbol{D}(t)||_2\\ &\leqslant -\frac{1}{2}\lambda_{Qc1}||\boldsymbol{w}_1||_2^2 - \left(\frac{1}{2}\epsilon\lambda_{Qo1} - \frac{2\lambda_{Fx2}}{\lambda_{Qc1}}\lambda_{Pc2}^2\right)||\boldsymbol{w}_2||_2^2 + \frac{2\epsilon}{\lambda_{Qo1}}\lambda_{Po2}^2||\boldsymbol{D}(t)||_2^2.\end{aligned} \tag{48}$$

With Assumption 1 in mind, it obtains from (48) that

$$\dot{V} \leqslant -k_1||\boldsymbol{w}_1||_2^2 - k_2||\boldsymbol{w}_2||_2^2 + k_3(k_{dm}^2 + k_{ds}^2), \tag{49}$$

with

$$k_1 = \frac{1}{2}\lambda_{Qc1}, \quad k_2 = \frac{1}{2}\epsilon\lambda_{Qo1} - \frac{2\lambda_{Fx2}}{\lambda_{Qc1}}\lambda_{Pc2}^2, \quad k_3 = \frac{2\epsilon}{\lambda_{Qo1}}\lambda_{Po2}^2.$$

It is obvious that $k_1 > 0$ and $k_3 > 0$. Since $\epsilon$ is a designed constant, $k_2 > 0$ is always established by designing a big enough $\epsilon$ in (43). Therefore, $V$ converges asymptotically until $k_1||\boldsymbol{w}_1||_2^2 + k_2||\boldsymbol{w}_2||_2^2 > k_3(k_{dm}^2 + k_{ds}^2)$ is not satisfied. Therefore, $\boldsymbol{w}_1$ and $\boldsymbol{w}_2$ converge to the following bounded region:

$$k_1||\boldsymbol{w}_1||_2^2 + k_2||\boldsymbol{w}_2||_2^2 \leqslant k_3(k_{dm}^2 + k_{ds}^2). \tag{50}$$

Therefore, the position and force tracking errors converge to a bounded region.

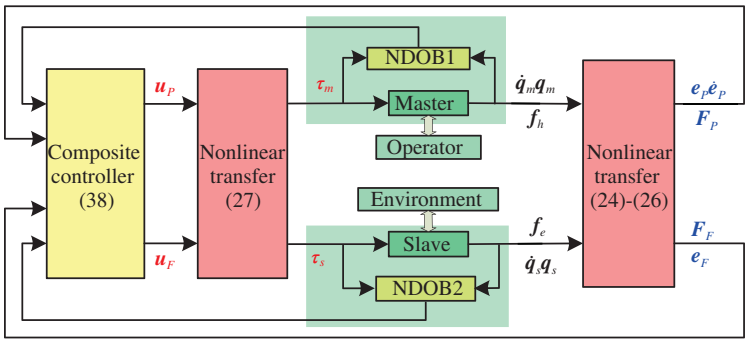


**Figure 3** (Color online) Block diagram of the nonlinear composite bilateral controller based on nonlinear disturbance observer.

**Theorem 4.** Suppose that Assumptions 1 and 2 are satisfied for the teleoperation system (1). The proposed nonlinear composite bilateral controller (38) guarantees the position and force tracking errors converge to zero asymptotically if the controller parameters are designed as $k_{PP} > 0$, $k_{PD} > 0$, $k_F > 0$ and the observer gains in (30) are designed as positive constants.

*Proof.* Since Assumption 1 is satisfied, it obtains from above proof that the dynamics (40) and (41) are input-to-state stable. It concludes from Assumption 2 and the definition in (41) that $\lim_{t\to\infty} \boldsymbol{D}(t) = \boldsymbol{0}$. Therefore, it can be derived from the ISS definition in [22] that $\boldsymbol{w}_1$ and $\boldsymbol{w}_2$ converge to zero asymptotically, i.e., the position and force tracking errors converge to zero asymptotically, which completes the proof.

The control structure of the proposed controller is given by Figure 3.

**Remark 4.** The proposed controller eliminates the influence of the nonlinear dynamics in position and force tracking error subsystems directly through the feedback of themselves while the WDOB and MDOB based composite controllers regard the nonlinear dynamics as disturbances and compensate them based on the estimations of LDOB. Consequently, the proposed controller has better position and force tracking performance than the WDOB and MDOB based composite controllers.

**Remark 5.** The proposed nonlinear composite bilateral controller attenuates the influence of disturbances in force and position tracking error dynamics through a feedforward compensation way which guarantees fast convergence rate. While the force tracking error dynamics under the WDOB and MDOB based composite bilateral controller in (16) and (22) couple with system states, their convergence is obtained through feedback regulation in a relatively slow way.

**Remark 6.** The ultimate bounds of the tracking errors denoted by (50) are determined by the controller parameters $k_{PD}$, $k_{PP}$, $k_F$, observer gains $l_{11}, \ldots, l_{1n}$, $l_{21}, \ldots, l_{2n}$ and the bounds of disturbance' derivatives $k_{dm}$, $k_{ds}$. The ultimate bounds of the tracking errors can be tuned small enough by choosing big controller parameters and observer gains.

## 5 Simulation analysis

To validate the effectiveness of the proposed nonlinear composite bilateral controller, simulations on a 2-DOF nonlinear teleoperation system are carried out in this section. The master and slave robots in this system are two-link revolute-joint robots and their mechanical structure is illustrated by Figure 4, where $l_{m1}$, $l_{m2}$, $l_{s1}$, $l_{s2}$ are the lengths of links, and $q_{m1}$, $q_{m2}$, $q_{s1}$, $q_{s2}$ are the 1st and 2nd joint angles of master and slave robots, respectively.

### 5.1 Model of 2-DOF nonlinear teleoperation system

The dynamics of 2-DOF nonlinear teleoperation system is the same with (1) for the case $n = 2$. Since both master and slave are two-link revolute-joint robots, they have the same structures i.e., $\boldsymbol{M}_m(\boldsymbol{q}_m)$ and $\boldsymbol{M}_s(\boldsymbol{q}_s)$, $\boldsymbol{C}_m(\boldsymbol{q}_m, \dot{\boldsymbol{q}}_m)$ and $\boldsymbol{C}_s(\boldsymbol{q}_s, \dot{\boldsymbol{q}}_s)$, $\boldsymbol{G}_m(\boldsymbol{q}_m)$ and $\boldsymbol{G}_s(\boldsymbol{q}_s)$ are the same functions in terms of joint

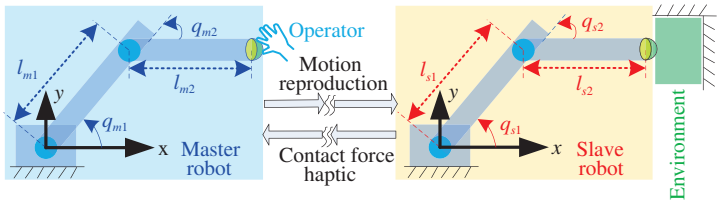


**Figure 4** (Color online) Mechanical structure of the two-link revolute-joint robot based teleoperation system.

**Table 1** Parameters of the master, slave, operator and environment

| Parameter | $m_{m1}$ | $m_{m2}$ | $l_{m1}$ | $l_{m2}$ | $m_{s1}$ | $m_{s2}$ | $l_{s1}$ | $l_{s2}$ | $b_h$ | $k_h$ | $b_e$ | $k_e$ |
|---|---|---|---|---|---|---|---|---|---|---|---|---|
| Unit | kg | kg | m | m | kg | kg | m | m | Ns/m | N/m | Ns/m | N/m |
| Value | 2 | 1 | 1 | 1 | 4.6 | 2.3 | 1 | 1 | 120 | 1500 | 50 | 1000 |

**Table 2** Controller formulations and parameters of different control methods

| Method | Controller formulations | Controller parameters | Observer gains |
|---|---|---|---|
| Proposed controller | Eqs. (30), (37) and (38) | $k_{PD}=40,\ k_{PP}=400,\ k_F=20$ | $l_{11}=l_{12}=l_{21}=l_{22}=100$ |
| MDOB based controller | Eqs. (13), (19) and (20) | $k_{PD}=40,\ k_{PP}=400,\ k_F=20$ | $\bar{g}_1=\bar{g}_2=\bar{g}_3=\bar{g}_4=100$ |
| WDOB based controller | Eqs. (9), (12) and (13) | $k_{PD}=40,\ k_{PP}=400,\ k_F=20$ | $g_m^1=g_m^2=g_s^1=g_s^2=100$ |
| Baseline NFL controller | Eq. (28) | $k_{PD}=40,\ k_{PP}=400,\ k_F=20$ | – |

angles. The dynamics of two-link revolute-joint robot are as follows [23]:

$$\boldsymbol{M}(\boldsymbol{q})=\begin{bmatrix} l_2^2m_2+2l_1l_2m_2c_2+l_1^2(m_1+m_2) & l_2^2m_2+l_1l_2m_2c_2 \\ l_2^2m_2+l_1l_2m_2c_2 & l_2^2m_2 \end{bmatrix},$$

$$\boldsymbol{C}(\boldsymbol{q},\dot{\boldsymbol{q}})=\begin{bmatrix} -2l_1l_2m_2s_2\dot{q}_2 & -l_1l_2m_2s_2\dot{q}_2 \\ l_1l_2m_2s_2\dot{q}_2 & 0 \end{bmatrix},\quad \boldsymbol{G}(\boldsymbol{q})=\begin{bmatrix} m_2l_2gc_{12}+(m_1+m_2)l_1gc_1 \\ m_2l_2gc_{12} \end{bmatrix},$$

where $m_1$, $m_2$ and $l_1$, $l_2$ are the masses and lengths of first and second robot's links, $s_1$, $s_2$, $c_1$, $c_2$, $s_{12}$, $c_{12}$ are the functions of joint angles as follows:

$$s_1=\sin(q_1),\ s_2=\sin(q_2),\ c_1=\cos(q_1),\ c_2=\cos(q_2),\ s_{12}=\sin(q_1+q_2),\ c_{12}=\cos(q_1+q_2).$$

For a two-link revolute-joint robot, the kinematics of its end effector position is the same with (2) for the case $r=2$ as

$$\boldsymbol{h}(\boldsymbol{q})=\begin{bmatrix} l_1c_1+l_2c_{12} \\ l_1s_1+l_2s_{12} \end{bmatrix},\qquad \boldsymbol{J}(\boldsymbol{q})=\begin{bmatrix} -l_1s_1-l_2s_{12} & -l_2s_{12} \\ l_1c_1+l_2c_{12} & l_2c_{12} \end{bmatrix}.$$

Let $m_{m1}$, $m_{m2}$ and $m_{s1}$, $m_{s2}$ denote the masses of master and slave robots' links respectively. The mechanical parameters of master and slave robots and the contact force parameters in (3) are set as Table 1 in the simulations. The human operator and environment exogenous forces are set as

$$\boldsymbol{f}_h^r=[f_{hx}^r\ f_{hy}^r]^{\mathrm{T}}=[15-20\cos(2\pi t)\ \ 10-20\sin(2\pi t)]^{\mathrm{T}},\qquad \boldsymbol{f}_e^r=[f_{ex}^r\ f_{ey}^r]^{\mathrm{T}}=[0\ \ 0]^{\mathrm{T}}.$$

### 5.2 Controller design and simulation scenario setting

To better demonstrate the merits of the proposed nonlinear composite bilateral controller, both the proposed controller and the composite bilateral controllers based on WDOB and MDOB are employed in the simulations. Besides, the baseline NFL controller is also employed in the simulations for comparisons. The controller formulations and parameters of different methods are designed and shown in Table 2.

The scaling constants for position and force in (6) are set as $\alpha=1$ and $\beta=0.5$, respectively. The initial angle positions of master and slave are set as $q_{m1}(0)=60^\circ$, $q_{m2}(0)=-60^\circ$ and $q_{s1}(0)=60^\circ$, $q_{s2}(0)=-55^\circ$, respectively. To make the operation tasks more challenging, three types of external disturbance torques are assumed to act on the teleoperation system in the simulations. The external disturbance torques $\boldsymbol{d}_m=[d_{m1}(t)\ d_{m2}(t)]^{\mathrm{T}}$, $\boldsymbol{d}_s=[d_{s1}(t)\ d_{s2}(t)]^{\mathrm{T}}$ in three cases are shown in Table 3.

**Table 3** External disturbance torques setting

| Disturbance type | Execution time | $d_{m1}(t)$ | $d_{m2}(t)$ | $d_{s1}(t)$ | $d_{s2}(t)$ |
|---|---|---|---|---|---|
| Disturbance free | $t \leqslant 2$ | 0 | 0 | 0 | 0 |
| Time-varying | $2 < t \leqslant 4$ | $10 - 5\sin(2t)$ | $10 + 5\sin(2t)$ | $20 - 10\sin(2t)$ | $20 + 10\sin(2t)$ |
| Constant | $4 < t \leqslant 6$ | 10 | 10 | 20 | 20 |

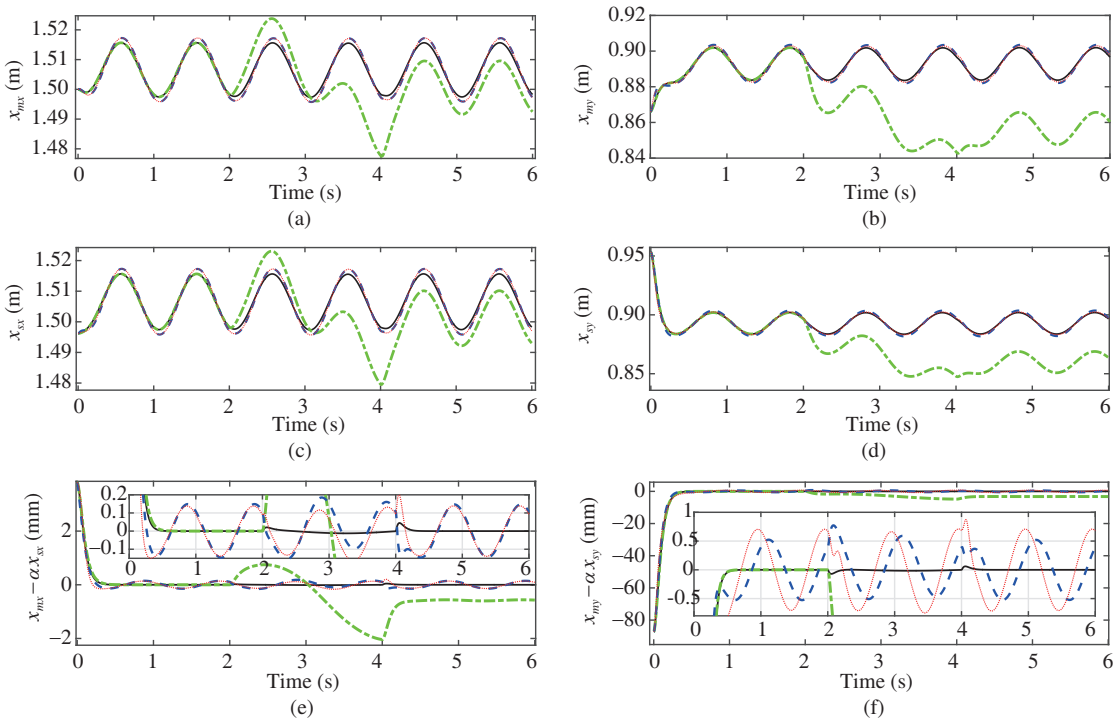


**Figure 5** (Color online) Response curves of end effector positions under the proposed controller (solid line), MDOB based composite controller (dashed line), WDOB based composite controller (dotted line) and baseline NFL controller (dash-dot line). (a) Position of master robot in $x$ axis; (b) position of master robot in $y$ axis; (c) position of slave robot in $x$ axis; (d) position of slave robot in $y$ axis; (e) position tracking error in $x$ axis; (f) position tracking error in $y$ axis.

### 5.3 Simulation results

Responses curves of the end effector positions and the trajectories of master and slave robots under the four control methods are given in Figures 5 and 6. Figures 7 and 8 demonstrate the response curves of contact forces and control actions of master and slave robots. To demonstrate the tracking performance more clearly, the response curves of position and force tracking errors in Figures 5(e), 5(f), 7(e) and 7(f) are zoomed in. In the following part, we will analyse the control performance of the teleoperation systems in the presence of different types of external disturbance torques.

**Disturbance free ($t \leqslant 2$).** It concludes from the response curves of position and force tracking errors in Figures 5(e), 5(f), 7(e) and 7(f) during slot $t \leqslant 2$ that: (1) Both the proposed controller and the baseline controller guarantee the asymptotical convergence of position and force tracking errors, while the MDOB based and the WDOB based composite controller only guarantee the tracking errors converge to a bounded region, which verifies the statement in Remark 4. (2) The tracking errors under MDOB based composite controller have a better dynamic response than that under the WDOB based composite controller as stated in Remark 1. The trajectories of the master and slave robots shown in Figures 6(a)–(d) clearly demonstrate that the proposed controller and the baseline controller have better position tracking performance than other methods due to the full utilization of the nonlinear dynamics in teleoperation systems. It can be observed from Figure 8 that the control actions under the four control methods are in the similar level and this denotes the fairness of the simulation comparison.

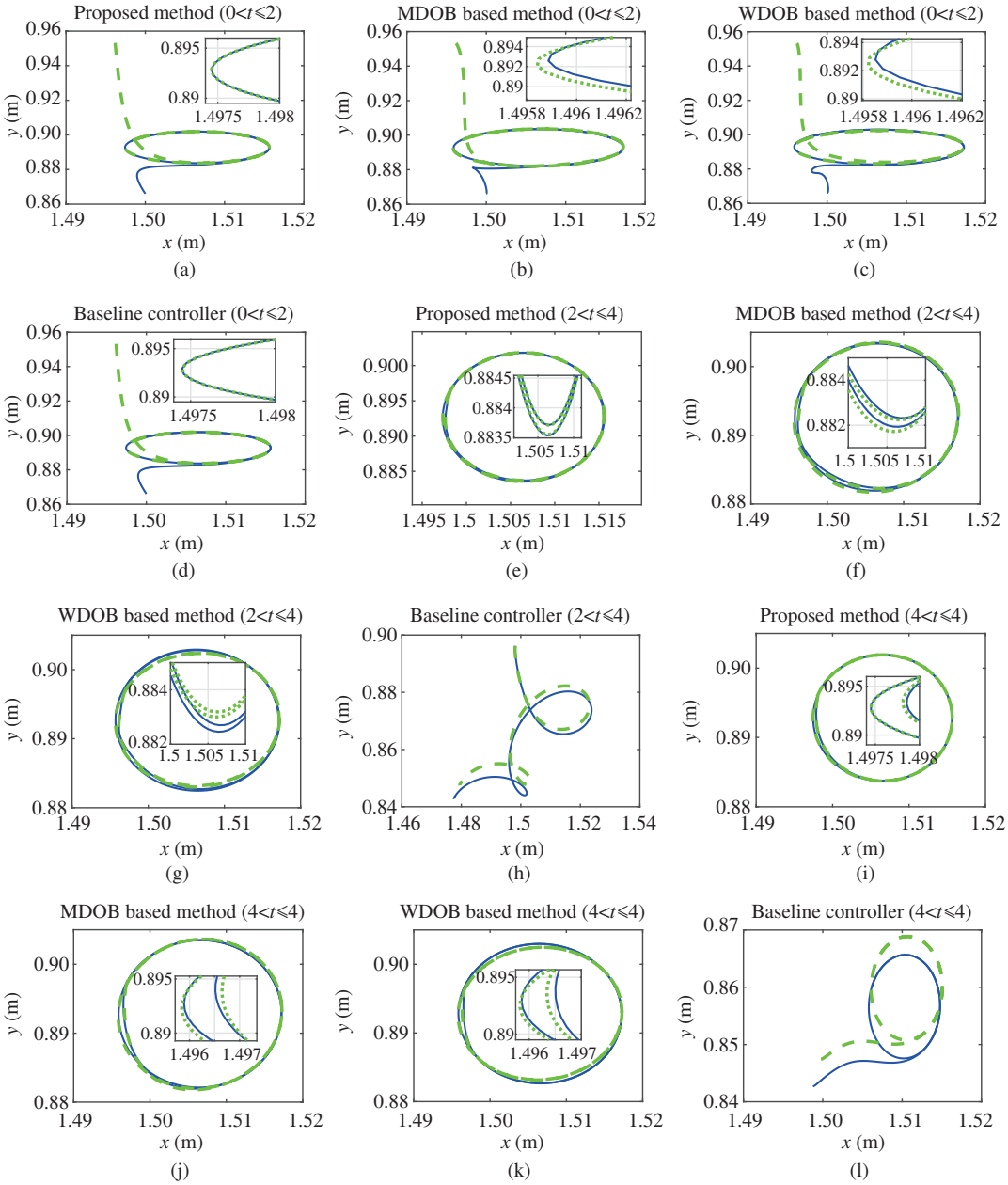


**Figure 6** (Color online) Trajectories of master robot (solid line) and slave robot (dotted line) with different types of disturbances under different controllers. (a)–(d) Without disturbances ($t \leqslant 2$): (a) proposed controller, (b) MDOB based controller, (c) WDOB based controller, (d) baseline controller. (e)–(h) With time-varying disturbances ($2 < t \leqslant 4$): (e) proposed controller, (f) MDOB based controller, (g) WDOB based controller, (h) baseline controller. (i)–(l) With constant disturbances ($4 < t \leqslant 6$): (i) proposed controller, (j) MDOB based controller, (k) WDOB based controller, (l) baseline controller.

**In the presence of time-varying disturbances ($2 < t \leqslant 4$).** It can be observed from the response curves of position and force tracking errors during $2 < t \leqslant 4$ in Figures 5(e) 5(f), 7(e) and 7(f) that: (1) The proposed controller guarantees the position and force tracking errors converge to a small bounded region in the presence of persistent bounded disturbances as stated in Theorem 3; (2) All the three composite controllers guarantee the position and force tracking errors converge to a bounded region, while the convergence region under the proposed controller is much smaller than other methods; (3) The ultimate bounds under the baseline controller are really large. It is observed from Figure 6(e)–(h) that the proposed controller has the best position tracking performance among the four control methods. It

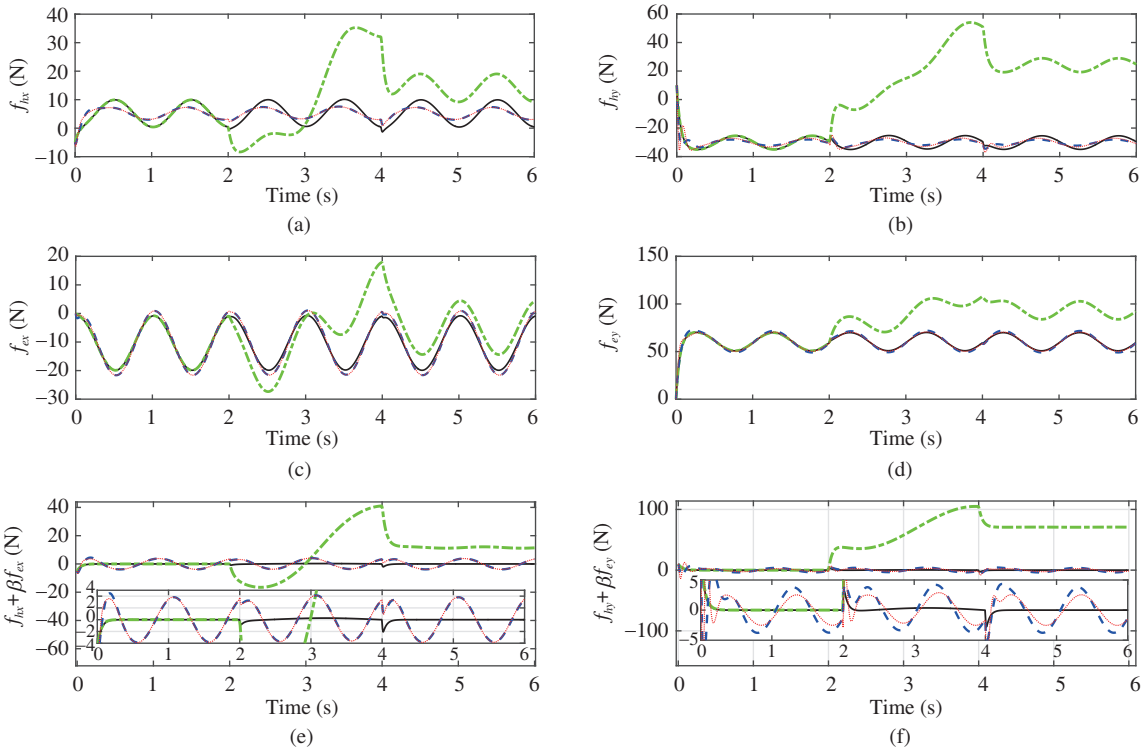


**Figure 7** (Color online) Response curves of contact forces under the proposed controller (solid line), MDOB based composite controller (dashed line), WDOB based composite controller (dotted line) and the baseline NFL controller (dash-dot line). (a) Force applied on master in $x$ axis; (b) force applied on master in $y$ axis; (c) force applied on slave in $x$ axis; (d) force applied on slave in $y$ axis; (e) force tracking error in $x$ axis; (f) force tracking error in $y$ axis.

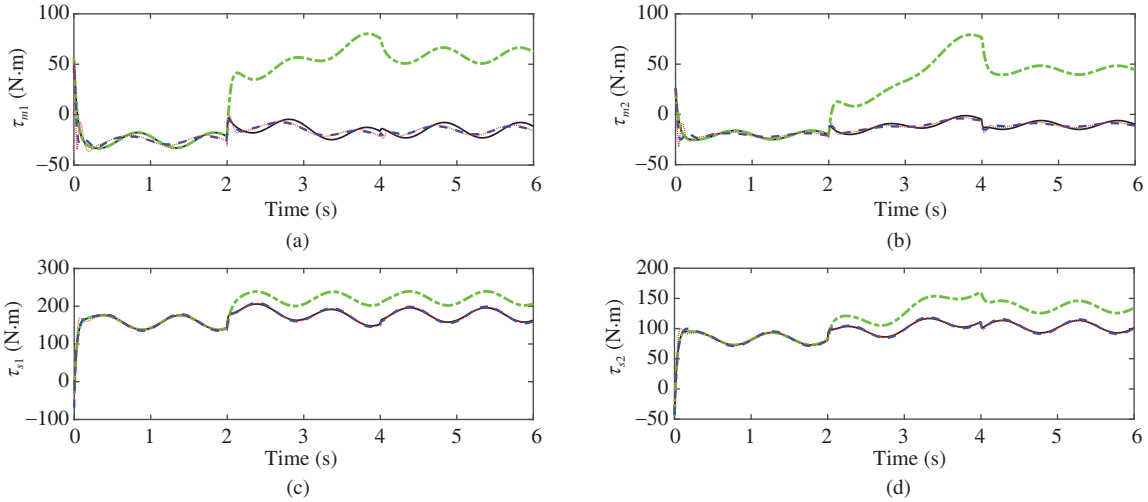


**Figure 8** (Color online) Response curves of control torques under the proposed controller (solid line), MDOB based composite controller (dashed line), WDOB based composite controller (dotted line) and the baseline NFL controller (dash-dot line). (a) Control torques of master robot in the first joint; (b) control torques of master robot in the second joint; (c) control torques of slave robot in the first joint; (d) control torques of slave robot in the second joint.

concludes from Figure 8 that the control actions of the four control methods are in the similar level.

**In the presence of constant disturbances ($4 < t \leqslant 6$).** The response curves of position and force tracking errors in Figures 5(e), 5(f), 7(e) and 7(f) during $4 < t \leqslant 6$ show that: (1) The proposed controller guarantees asymptotical convergence of position and force tracking errors as stated in Theorem 4; (2) Both the MDOB based and WDOB based composite controllers only guarantee position and force tracking errors converge to a bounded region; (3) The baseline controller results in large offset tracking errors.

Figures 6(i)–(l) show that the proposed controller has the highest position tracking precision among the four control methods. Figure 8 illustrates the fairness of the simulation comparison.

## 6 Conclusion

This paper has investigated the bilateral control problem of n-DOF nonlinear teleoperation systems with external disturbances. Two existing well established linear disturbance observer based composite bilateral control methods have been given and analysed in detail at first. Motivated by their shortcomings, a new nonlinear composite control method has been developed based on the nonlinear disturbance observer. It has been shown that the proposed control method guarantees satisfactory motion reproduction and remote force haptic simultaneously for the n-DOF teleoperation systems with external disturbances. Simulation results of a 2-DOF teleoperation systems have validated the effectiveness of the proposed control method. Further work would focus on the estimation methods of contact force and the experimental investigations of them. Considering the successful applications of composite learning methods [24, 25], we will also explore how these methods perform on the bilateral systems in the future research.

**Acknowledgements** This work was supported by National Natural Science Foundation of China (Grant Nos. 61473080, 61573099, 61633003, 61750110525), Fundamental Research Funds for Central Universities (Grant No. 2242016R30011), Graduate Innovation Program of Jiangsu Province (Grant No. KYLX15-0114), Scientific Research Foundation of Graduate School of Southeast University (Grant No. YBJJ1561) and Open Project Program of Ministry of Education Key Laboratory of Measurement and Control of CSE (Grant No. MCCSE2017A01). Zhenhua ZHAO would also like to thank Chinese Scholarship Council and Newton Fund by British Council for supporting his study in the UK.

### References

1 Daly J M, Wang D W L. Time-delayed output feedback bilateral teleoperation with force estimation for $n$-DOF nonlinear manipulators. IEEE Trans Contr Syst Technol, 2014, 22: 299–306
2 Zhang B, Li H Y, Tang G J. Human control model in teleoperation rendezvous. Sci China Inf Sci, 2014, 57: 112205
3 Peng L, Hou Z G, Peng L, et al. Robot assisted rehabilitation of the arm after stroke: prototype design and clinical evaluation. Sci China Inf Sci, 2017, 60: 073201
4 Lawrence D A. Stability and transparency in bilateral teleoperation. IEEE Trans Robot Automat, 1993, 9: 624–637
5 Hannaford B. A design framework for teleoperators with kinesthetic feedback. IEEE Trans Robot Automat, 1989, 5: 426–434
6 Tavakoli M, Aziminejad A, Patel R V, et al. High-fidelity bilateral teleoperation systems and the effect of multimodal haptics. IEEE Trans Syst Man Cybern B, 2007, 37: 1512–1528
7 Zhai D H, Xia Y. Adaptive control for teleoperation system with varying time delays and input saturation constraints. IEEE Trans Ind Electron, 2016, 63: 6921–6929
8 Zhai D H, Xia Y. Finite-time control of teleoperation systems with input saturation and varying time delays. IEEE Trans Syst Man Cybern: Syst, 2017, 40: 1522–1534
9 Yang Y, Hua C, Guan X. Finite time control design for bilateral teleoperation system with position synchronization error constrained. IEEE Trans Cybern, 2016, 46: 609–619
10 Matsumoto Y, Katsura S, Ohnishi K. An analysis and design of bilateral control based on disturbance observer. In: Proceedings of the IEEE International Conference on Industrial Technology, Maribor, 2003. 802–807
11 Sakaino S, Sato T, Ohnishi K. Multi-DOF micro-macro bilateral controller using oblique coordinate control. IEEE Trans Ind Inf, 2011, 7: 446–454
12 Nozaki T, Mizoguchi A, Ohnishi K. Decoupling strategy for position and force control based on modal space disturbance observer. IEEE Trans Ind Electron, 2014, 61: 1022–1032
13 Ohishi K, Ohnishi K, Miyachi K. Torque-speed regulation of dc motor based on load torque estimation. In: Proceedings of the Institute of Electrical Engineers of Japan, Tokyo, 1983. 1209–1216
14 Chen W-H, Ballance D J, Gawthrop P J, et al. A nonlinear disturbance observer for robotic manipulators. IEEE Trans Ind Electron, 2000, 47: 932–938
15 Sun N, Fang Y, Zhang X. Energy coupling output feedback control of 4-DOF underactuated cranes with saturated inputs. Automatica, 2013, 49: 1318–1325
16 Li S H, Yang J, Chen W-H, et al. Generalized extended state observer based control for systems with mismatched uncertainties. IEEE Trans Ind Electron, 2012, 59: 4792–4802
17 Yang J, Li S H, Yu X H. Sliding-mode control for systems with mismatched uncertainties via a disturbance observer. IEEE Trans Ind Electron, 2013, 60: 160–169

18 Sun H, Li Y, Zong G, et al. Disturbance attenuation and rejection for stochastic Markovian jump system with partially known transition probabilities. Automatica, 2018, 89: 349–357
19 Mohammadi A, Tavakoli M, Marquez H J. Disturbance observer-based control of non-linear haptic teleoperation systems. IET Control Theor Appl, 2011, 5: 2063–2074
20 Mohammadi A, Marquez H J, Tavakoli M. Nonlinear disturbance observers: design and applications to Euler-Lagrange systems. IEEE Control Syst, 2017, 37: 50–72
21 Li S H, Yang J, Chen W-H, et al. Disturbance Observer-based Control: Methods and Applications. Boca Raton FL: CRC Press, 2014. 14–17
22 Khalil H K. Noninear Systems. 2nd. New Jersey: Prentice-Hall, 1996. 174–180
23 Kelly R, Santibanez V, Loriá A. Control of Robot Manipulators in Joint Space. Berlin: Springer, 2005. 95–110
24 Pan Y, Yu H. Composite learning from adaptive dynamic surface control. IEEE Trans Automat Contr, 2016, 61: 2603–2609
25 Xu B, Sun F, Pan Y, et al. Disturbance observer based composite learning fuzzy control of nonlinear systems with unknown dead zone. IEEE Trans Syst Man Cybern Syst, 2017, 47: 1854–1862